JOURNAL OF GEOPHYSICAL RESEARCH, VOL. 106, NO. D1, PAGES 1249–1269, JANUARY 16, 2001

A microphysics-based investigation of the radiative effects of aerosol-cloud interactions for two MAST Experiment case studies

Carynelisa Erlick[1]

Atmospheric and Oceanic Sciences Program, Princeton University, Princeton, New Jersey

Lynn M. Russell

Department of Chemical Engineering, Princeton University, Princeton, New Jersey

V. Ramaswamy

Geophysical Fluid Dynamics Laboratory, Princeton University, Princeton, New Jersey

Abstract. We use a size- and composition-resolved externally mixed aerosol microphysical model and a delta-Eddington exponential-sum-fit radiation algorithm to examine the interactions between aerosol particles and cloud drops, and their influence on solar radiation. Both the aerosol model and the radiation code are designed to explicitly handle external and internal aerosol particle and cloud drop mixtures. Using observations from the Monterey Area Ship Track (MAST) Experiment, we model changes in aerosol and cloud drop size distributions for a clean marine cloud and ship track and a continentally influenced marine cloud and ship track. Linking these results to the radiation algorithm with a Mie-scattering subroutine, we investigate the corresponding changes in cloud albedo, cloud absorption, and transmission. The differences in 0.3–3.0 μm albedo and transmission between the clouds and ship tracks as a result of the changes in drop size distribution and composition are found to be substantial, and the composition of the cloud drops is found to be important particularly in the continentally influenced case. Both the clouds and ship tracks enhance atmospheric absorption with respect to a clear sky, with a cloud forcing ratio ranging from 1.15 to 1.37, where the clear sky is defined to be cloud- and aerosol-free. Sensitivity studies are performed with respect to the updraft velocity, the updraft area fraction, dilution of the ship emissions, and the composition of supermicron continental particles. The radiation results are also compared with Meteorological Research Flight (MRF) C-130 in situ aircraft measurements and with parameterizations of the "Twomey effect."

1. Introduction

The suggestion by *Twomey* [1974] that increases in anthropogenic aerosol concentrations can lead to increases in the solar reflectivity of clouds has been confirmed by a number of studies using both parameterized models and in situ and remote sensing observations [e.g., *Fitzgerald and Spyers-Duran*, 1973; *Kondratyev*, 1981; *Twomey et al.*, 1984; *Pueschel et al.*, 1986; *Radke et al.*, 1989; *Leaitch et al.*, 1992; *Alkezweeny et al.*, 1993; *King et al.*, 1993; *Jones et al.*, 1994; *Twohy et al.*, 1995, *Feichter et al.*, 1997; *Ferek et al.*, 1998]. These studies relate increases in cloud condensation nuclei to cloud drop concentration, effective or mean droplet radius, and cloud albedo. However, certain issues which are also likely to be important in a global assessment of the "Twomey effect," such as changes in liquid water content, the role of unactivated interstitial aerosols, and effects involving cloud absorption and transmission, have not been fully addressed. In this work, we use observations from the Monterey Area Ship Track (MAST) Experiment [*Durkee et al.*, 2000b; *Hobbs et al.*, 2000; *Russell et al.*, 1999] together with a size- and composition-resolved externally mixed aerosol model [*Russell and Seinfeld*, 1998] and a delta-Eddington exponential-sum-fit solar radiation algorithm [*Freidenreich and Ra-*

[1]Now at Ring Department of Atmospheric Sciences, The Hebrew University of Jerusalem, Jerusalem, Israel.

Paper number 2000JD900567.
0148-0227/01/2000JD900567$09.00

maswamy, 1999] to investigate in a detailed microphysical manner the changes in cloud albedo, absorption, and transmission as a consequence of ship-emitted aerosol particles. Using observations and models in a joint fashion and explicitly describing the aerosol and cloud drop distributions, we are able to differentiate particle size and composition effects on the radiation field.

The ability to keep track of the particle size and composition during cloud evolution, while it limits the scale of the aerosol model to a parcel model, has a unique advantage over larger-scale models. Mesoscale models and general circulation models (GCMs), which include microphysics, do so in a parameterized manner and usually only as a function of sulfate amount [*Reisin et al.*, 1996; *Ghan et al.*, 1997; *Lohmann and Feichter*, 1997]. While these capture the interaction between the nucleation of sulfate aerosols and dynamics on some scale, they cannot describe the influences of other compositions on the cloud drop spectrum. Furthermore, since they are unable to resolve mixtures of masses of different chemical species within droplets, they cannot unambigously describe the influences of the different compositions on the radiative properties of clouds. By embedding the size- and composition-resolved aerosol model in a one-dimensional (1-D) Eulerian profile constrained by observations, we are able to test the importance of different microphysical parameters on the radiative properties of clouds. This type of model is the only means available at this time to investigate the competing effects of different aerosol types in cloud evolution in such a chemically and microphysically rigorous representation [*Russell et al.*, 1999].

2. Description of the Models Used

The aerosol model of *Russell and Seinfeld* [1998] is a parcel model embedded in a vertical profile of temperature, pressure, and relative humidity. It predicts the growth of aerosol populations for explicit external and internal mixtures of aerosol species, accounting for the processes of coagulation, condensation, deposition, activation, and nucleation. For nonwater components, a fixed sectional representation of the size domain is used, where both particle number and mass are conserved as particles grow from one section to the next. During coagulation between different aerosol populations, the identity of the coagulated particles remains with the characteristic involatile core. Water condensation is treated with a moving sectional representation of the size domain, where the unactivated section divisions are retained during activation so that particles of different origin are not lumped into a single activated size class. Maximum supersaturation, ultimate drop size, and number of droplets formed are determined by kinetic rather than equilibrium Köhler theory. This is more realistic particularly in warm stratus clouds where the rate of change of the supersaturation can be comparable to or faster than the rate of particle growth. These algorithms provide accurate tracking of multiple particle populations under changing supersaturation conditions. A more detailed description is given by *Russell et al.* [1999].

The aerosol particles are divided into four types based on their source: DMS-derived nonsea salt sulfate (hereafter abbreviated as nss-sulfate), sea salt, ship plume, and continental. These four types are in turn comprised of internal mixtures of six species: water, ammonium sulfate, ammonium bisulfate, sodium chloride, organic carbon, and black carbon. Mie scattering parameters for each aerosol type are computed with the Mie scattering subroutine for homogeneous spheres from *Bohren and Huffman* [1983, appendix A]. The composite refractive index for each aerosol type is calculated using a volume-weighted linear mixing rule [*Hänel*, 1976, equation (2.49)] for the nonabsorbing species and Maxwell-Garnett theory [*Bohren and Huffman*, 1983, section 8.5] for organic and black carbon.

Refractive indices for each species as a function of wavelength are derived from various sources. The real and imaginary parts of the refractive indices for water are from *Hale and Querry* [1973]. The aqueous real part of the refractive index for ammonium sulfate uses an extrapolation to 100% weight solute of data from *Weast et al.* [1985–1986, p. D-233], where the wavelength dependence matches that of water. The imaginary part of the refractive index for ammonium sulfate is from *Toon* [1976]. The same is true for ammonium bisulfate, where the extrapolation to 100% weight solute uses data from *Tang and Munkelwitz* [1994], and for sodium chloride, where the extrapolation to 100% weight solute uses data from *Weast et al.* [1985–1986, pp. D-253–D-254]. The real part of the refractive index for organic carbon is calculated based on the value for octacosanoic acid at 550 nm from *Weast et al.* [1985–1986, p. C-380], where the wavelength dependence matches that of water. The imaginary part of the refractive index for organic carbon is the imaginary part of the refractive index for water-soluble components (consisting of sulfates, nitrates, and soluble organics) from *d'Almeida et al.* [1991, Table 4.3]. The real and imaginary parts of the refractive indices for black carbon and dust are from *d'Almeida et al.* [1991, Table 4.3], matching those for soot and dry desert mineral dust.

Given the composite refractive indices for each aerosol type in each size bin in each atmospheric layer and the accompanying size distributions, the Mie-scattering subroutine provides the extinction optical depths, single-scattering albedos, and asymmetry factors as a function of wavelength. These then act as inputs to the radiation algorithm, a 26-band solar parameterization for inhomogeneous scattering and absorbing atmospheres, spanning wavenumbers 0 – 57,600 cm^{-1} and wavelengths 0.174 μm to greater than 4.0 μm. For details see *Freidenreich and Ramaswamy* [1999]; only a brief description is given here. The algorithm was developed from line-by-line and doubling-adding reference

computations with particular emphasis on accurately representing atmospheric absorption when both clouds and water vapor are present. The model atmosphere contains 158 pressure levels, with 50-m layers up to 2000 m altitude, 200-m layers from 2000 to 7000 m altitude, and layers 20-mbar thick or less up to the top of the atmosphere. The exponential sum-fit technique [*Wiscombe and Evans*, 1977] is used for the parameterization of water vapor transmission in the main absorbing bands, where average transmission in a band is expressed as a series expansion of terms exponential in water vapor amount. The expansion coefficients and coefficients of the water vapor amount are fitted to the line-by-line-derived heating rate profile using a least squares routine. Absorption by other gases (CO_2, O_2, and O_3) is computed using a regular absorptivity approach, where the transmission in a band is 1 minus the absorption and the absorption is a function of the absorber amount. The coefficients in the expressions for the CO_2, O_2, and O_3 absorption are also fitted to the reference heating rate profile. The delta-Eddington method [*Joseph et al.*, 1976] is used to calculate the reflection and transmission of scattering layers, accounting for scattering and absorption by molecules, aerosol particles, and cloud drops, and the layers are combined using the adding method [*Ramaswamy and Bowen*, 1994]. The algorithm is structured to be suitable for use in atmospheric GCMs, while accurately representing cloud absorption, stratospheric heating, and scattering and absorption by multiple atmospheric constituents.

The direct surface albedo is calculated using *Taylor et al.* [1996, equation (3)], which is derived from an ensemble of observations from the Meteorological Research Flight (MRF) C-130:

$$A_{\text{surf}} = \frac{0.037}{1.1\mu_0^{1.4} + 0.15}, \quad (1)$$

where μ_0 is the cosine of the solar zenith angle. The diffuse albedo is calculated as the integral of A_{surf} over zenith angle.

3. Observations From MAST

We consider two case studies from the Monterey Area Ship Track Experiment, which took place off the coast of Monterey, California (34°–39°N latitude, between 126°W longitude and the California coast), in June 1994 [*Russell et al.*, 1996; *Durkee et al.*, 2000b; *Noone et al.*, 2000a,b; *Hobbs et al.*, 2000; *Taylor et al.*, 2000]. (1) The bulk carrier *Star Livorno* was sampled by the University of Washington (UW) C131-A flight 1648 on June 29 (case JDT180), in a clean marine stratocumulus cloud extending from 230 m to a temperature inversion at 450 m altitude [*Hobbs et al.*, 2000]. (2) The container ship *Tai He* was sampled by UW C131-A flight 1646 on June 27 (case JDT178), in continentally influenced marine stratocumulus cloud extending from 173 m to a temperature inversion at 405 m altitude [*Noone et al.*, 2000b; *Hobbs et al.*, 2000]. These provide two extreme cases of clean and continentally influenced preship track maritime clouds and the corresponding influence of ship plume particles on their microphysics. They were studied primarily with instrumentation aboard the UW C-131A aircraft, which provided in-cloud thermodynamic measurements (average liquid water content, boundary layer height, ambient and dew point temperature profiles, and wind speed), particle number and size distribution measurements, and vapor measurements (SO_2, NO_x, O_3, and water vapor) [*Russell et al.*, 1995, 1996; *Hobbs et al.*, 2000]. In addition, the MRF C-130 aircraft flew near similar tracks in adjacent regions on the same days, and provided above-cloud thermodynamic measurements (temperature and dew point temperature profiles) and pyranometer measurements (295 nm to 3.0 μm irradiance and 715 nm to 3.0 μm irradiance) up to an altitude of ~7000 m [*Hobbs et al.*, 2000]. Above 7000 m, a midlatitude summer atmospheric profile [*McClatchey et al.*, 1972] is assumed in the radiation code.

For each simulation, the supersaturation rate is calculated based on the measured lapse rate and updraft velocity, where $dS/dt = wdS/dz$. Given the initial measured particle size distribution, the sea salt flux is calculated from the measured wind speed [*Bowyer et al.*, 1990; *Bigg et al.*, 1995], and the remaining clean marine submicron particles are assigned to nss-sulfate. The difference between the total plume particle number size distribution and the total background size distribution for each case is assigned to plume particles, where the plume particle distribution measurement is chosen closest to ship stack [*Russell et al.*, 1999]. Similarly, the difference between the background size distribution of the continentally influenced case and that of the clean marine case is assigned to continental particles. Sulfate-to-carbon and organic-carbon-to-black-carbon mass ratios are based on *Hildemann et al.* [1991], while mixing ratios of NH_3, H_2O_2, DMS, and H_2SO_4 are based on marine boundary layer concentrations [*Russell et al.*, 1999]. OH is calculated from measurements of NO_x, O_3, and UV irradiance, and the photochemical reaction constants for the oxidation of sulfur species are given by *Russell et al.* [1994].

4. Results

4.1. Clean Marine Case, *Star Livorno*, June 29 (JDT180a and JDT180t)

Figure 1 shows the cloud average size distributions (averaged over cloud depth) for the updraft regions of the clean marine stratocumulus ambient cloud and ship track, respectively. The size distributions for the downdraft regions of the clean marine ambient cloud and ship track (not shown here), which remain largely subsaturated (relative humidities ~96–99%), peak at diameters (D) below 1 μm, but have tails extending to

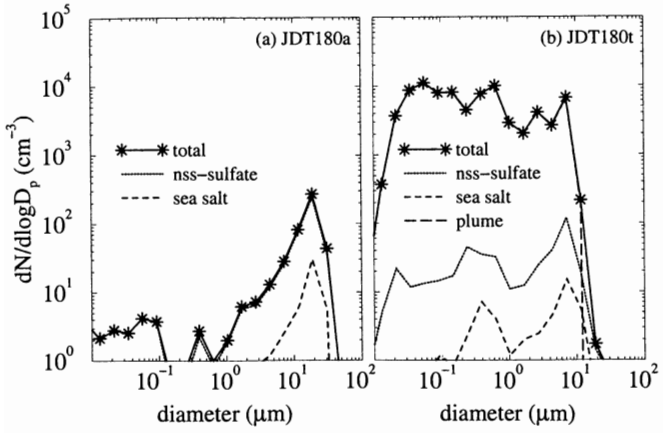

Figure 1. Updraft size distributions for the (a) clean marine ambient cloud (JDT180a) (liquid water content (LWC) = 0.19 g m^{-3}, r_{eff} = 10.8 μm) and (b) clean marine track (JDT180t) (LWC = 0.20 g m^{-3}, r_{eff} = 3.4 μm).

4–5 μm. Table 1 lists 550 nm extinction optical depths divided according to aerosol type and size. There are three size categories, $D < 1$ μm, $1 \leq D \leq 7$ μm, and $D > 7$ μm, chosen to represent particles, haze or small droplets, and activated or larger droplets, respectively. There are also three sets of optical depths in Table 1, corresponding to the updraft only region, the downdraft only region, and a 55% updraft/45% downdraft composite. The updraft only region has the highest optical depths, while the downdraft only region because it remains largely subsaturated has the lowest optical depths. In the 55% updraft/45% downdraft composite, the total optical depth of the clean marine cloud increases by more than a factor of 3 from 7.17 in the ambient cloud to 22.89 in the ship track. The largest contribution to the track optical depth is from activated plume particles in the 1–7 μm diameter range. Because the plume particles have grown by sulfate condensation on reaching cloud base such that their size distribution peaks at a larger diameter than that of the nss-sulfate aerosols, they are preferentially activated at the expense of the nss-sulfate particles, whose optical depth decreases accordingly from 6.40 in the ambient cloud to 0.43 in the ship track. The high number concentration of plume particles precludes them from growing into the > 7 μm size category, lowering the cloud average effective radius (volume averaged to area averaged radius; see equation (11)) from 10.8 to 3.4 μm.

As would be expected, the increase in number density and decrease in effective radius combines to increase the track optical depth. However, there is also a contribution from the liquid water content (LWC), which increases from 0.19 g m^{-3} in the ambient cloud to 0.20 g m^{-3} (~5% increase) in the ship track, creating an even higher track optical depth than would be predicted by conventional Twomey theory [*Twomey*, 1974; *Twomey et al.*, 1984]. (Note that this is a modeled rather than a measured increase in LWC. While some measurements from MAST also indicate an increase in LWC, the results are ambiguous, perhaps because of high spatial and temporal variability [*Noone et al.*, 2000a].) This increase in LWC is consistent with the results of *Fitzgerald and Spyers-Duran* [1973], *Pueschel et al.* [1986], *Radke et al.* [1989], *Leaitch et al.* [1992],

Table 1. Predicted Size-Differentiated 0.55 μm Extinction Optical Depths for the Clean Marine Ambient Cloud and Track, 0% Dilution

	Ambient Cloud, JDT180a			Track, JDT180t		
Aerosol type	$D < 1$ μm	$1 \leq D \leq 7$ μm	$D > 7$ μm	$D < 1$ μm	$1 \leq D \leq 7$ μm	$D > 7$ μm
			Updraft[a]			
Nss-sulfate	2×10^{-3}	0.06	11.59	4×10^{-3}	0.18	0.77
Sea salt	5×10^{-4}	9×10^{-3}	1.32	8×10^{-4}	0.02	0.13
Plume	—	—	—	0.61	13.00	26.84
			Downdraft[b]			
Nss-sulfate	8×10^{-3}	7×10^{-3}	0.05	3×10^{-3}	5×10^{-3}	0.02
Sea salt	1×10^{-3}	2×10^{-3}	1×10^{-5}	9×10^{-4}	2×10^{-3}	6×10^{-6}
Plume	—	—	—	0.06	3×10^{-7}	8×10^{-10}
			55% Updraft/45% Downdraft[c]			
Nss-sulfate	5×10^{-3}	0.04	6.40	3×10^{-3}	0.10	0.43
Sea salt	8×10^{-4}	6×10^{-3}	0.72	8×10^{-4}	0.01	0.07
Plume	—	—	—	0.37	7.15	14.76

[a]Ambient cloud total optical depth is 12.98. Track total optical depth is 41.55.
[b]Ambient cloud total optical depth is 0.07. Track total optical depth is 0.09.
[c]Ambient cloud total optical depth is 7.17. Track total optical depth is 22.89.

Table 2. Predicted Albedo, Absorption, and Transmission of the Clean Marine Ambient Cloud and Track for 55% Updraft/45% Downdraft and 0% Dilution

	Ambient Cloud, JDT180a		Track, JDT180t	
	All Species	Pure Water	All Species	Pure Water
Albedo	0.361	0.360	0.673	0.674
Absorption, W m^{-2}	39.0	39.0	45.5	41.6
Transmission	0.623	0.623	0.277	0.280

Here the albedo is simulated MRF C-130 broadband radiometer albedo, defined at altitude 1000 m, solar zenith angle 25.5°, and wavelength 0.3–3.0 μm. Absorption and transmission are calculated for the same solar zenith angle and wavelength.

Alkezweeny et al. [1993], *King et al.* [1993], and *Twohy et al.* [1995], although *Ferek et al.* [1998] did not find any ship track induced LWC increase. *Radke et al.* [1989] and *Ferek et al.* [1998] have suggested that an increase in LWC may be caused by the shift to smaller droplet radii, which suppresses drizzle and allows more liquid water to build up in the track. Table 1 also shows that particles with $D < 1$ μm contribute less than 1% to the total cloud optical depth, indicating that unactivated aerosol particles have little influence on the optical properties of the clean marine cloud in comparison with the larger activated aerosols.

Table 2 shows the predicted albedo, absorption, and transmission of the clean marine cloud and ship track. The wavelength region corresponds to MRF C-130 "clear band" radiometer measurements, where the albedo is defined at 1000 m altitude, the solar zenith angle is 25.5°, and the wavelength region is 0.3–3.0 μm. Note that since the albedo is defined at 1000 m here and throughout the paper, it incorporates to some extent multiple-scattering effects between the cloud and the surface and between the cloud and Rayleigh-scattering molecules above the cloud. A solar constant of 1358 W m^{-2} is used for all of the radiative transfer calculations.

As shown in Table 2, the increase in total optical depth from the clean marine ambient cloud to the ship track translates into an almost doubling of the clean marine cloud's predicted albedo, from 0.361 to 0.673. Absorbed irradiance increases from 39.0 W m^{-2} in the ambient cloud to 45.5 W m^{-2} in the ship track, and transmission decreases from 0.623 to 0.277. The absorbed irradiance may be compared to the average column absorption measured by *Evans et al.* [1995] under heavy clouds (50 W m^{-2}) and the global average reported by *Cess et al.* [1995] and *Ramanathan et al.* [1995] of > 25 W m^{-2}. (See section 5 for more on cloud absorption.)

To see how much effect the absorbing aerosol species have on the radiative properties of the cloud, the same calculations have been performed on a pure water cloud, where the indices of refraction have been changed to those of pure water but the size distributions have been held constant. (Near infrared absorption by water is taken into account in both the pure water and in the all-species calculations.) These results are also shown in Table 2. In the ambient cloud, there is very little difference between the pure water cloud and the all-species cloud. However, in the ship track, there is slightly less absorption in the pure water cloud than in the all-species cloud, which manifests itself in a slightly higher albedo and transmission. Clearly, the radiative properties of this clean marine stratocumulus are dominated by activated particles, whose water content swamps the absorbing contribution from residual aerosol species. (See section 5.)

4.2. Continentally Influenced Case, *Tai He*, June 27 (JDT178a and JDT178t)

Figure 2 shows the cloud average size distributions for the updraft regions of the continentally influenced marine stratocumulus cloud and ship track, respectively. The size distributions for the downdraft regions of the continentally influenced ambient cloud and ship track (not shown here) peak at diameters (D) below 1 μm but have tails extending to 11–12 μm. Table 3 lists the 550 nm extinction optical depths divided according to aerosol type and size. Here continental and plume

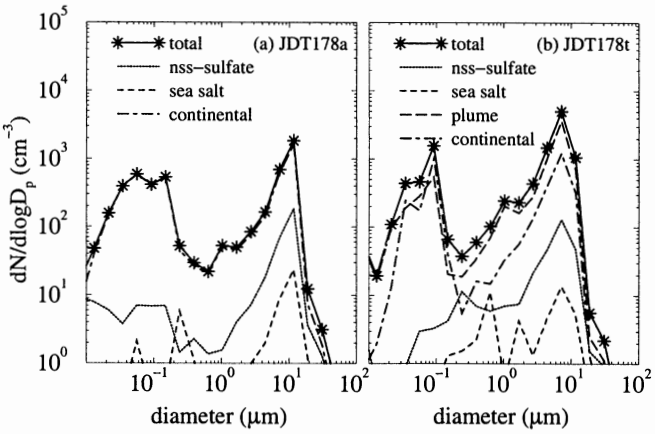

Figure 2. Updraft size distributions for the (a) continentally influenced ambient cloud (JDT178a) (LWC = 0.21 g m^{-3}, r_{eff} = 5.8 μm) and (b) continentally influenced track (JDT178t) (LWC = 0.22 g m^{-3}, r_{eff} = 4.1 μm).

Table 3. Predicted Size-Differentiated 0.55 μm Extinction Optical Depths for the Continentally Influenced Ambient Cloud and Track, 0% Dilution and Dust Supermicron Particle Composition

	Ambient Cloud, JDT178a			Track, JDT178t		
Aerosol type	$D < 1$ μm	$1 \leq D \leq 7$ μm	$D > 7$ μm	$D < 1$ μm	$1 \leq D \leq 7$ μm	$D > 7$ μm
			Updraft[a]			
Nss-sulfate	4×10^{-3}	0.10	2.82	6×10^{-3}	0.22	1.20
Sea salt	5×10^{-4}	0.01	0.36	1×10^{-3}	0.03	0.12
Plume	—	—	—	0.09	4.76	22.77
Continental	0.03	0.65	22.42	0.06	2.23	8.07
			Downdraft[b]			
Nss-sulfate	0.01	0.01	0.08	0.02	0.02	0.05
Sea salt	1×10^{-3}	4×10^{-3}	4×10^{-4}	1×10^{-3}	4×10^{-3}	3×10^{-4}
Plume	—	—	—	0.36	0.06	0.07
Continental	0.08	0.03	0.10	0.13	0.06	7×10^{-3}
			55% Updraft/45% Downdraft[c]			
Nss-sulfate	8×10^{-3}	0.06	1.59	0.01	0.13	0.68
Sea salt	7×10^{-4}	8×10^{-3}	0.20	1×10^{-3}	0.02	0.07
Plume	—	—	—	0.21	2.64	12.55
Continental	0.05	0.37	12.38	0.09	1.26	4.44

[a] Ambient cloud total optical depth is 26.39. Track total optical depth is 39.56.
[b] Ambient cloud total optical depth is 0.32. Track total optical depth is 0.78.
[c] Ambient cloud total optical depth is 14.67. Track total optical depth is 22.10.

aerosols are differentiated by their size distribution and by their sulfate-to-carbon mass ratios; the continental aerosols, which have aged, have a higher sulfate content. Like the clean marine stratocumulus, the updraft only region has the highest optical depths, while the downdraft only region which remains largely subsaturated has the lowest optical depths. However, in contrast to the clean marine cloud, the 55% updraft/45% downdraft total optical depth increases by only 50% from 14.67 in the continentally influenced ambient cloud to 22.10 in the ship track. The continental case is seen to have lesser effects due to the ship plume than the clean marine cloud, a feature that is consistent with the notion from earlier studies [e.g., *Platnick and Twomey*, 1994; *Taylor and McHaffie*, 1994; *Houghton et al.*, 1996; *Taylor et al.*, 2000], owing to the effects of a higher initial aerosol concentration in the airflow from continents. In the ambient cloud the largest contribution to the optical depth is from activated continental aerosols in the > 7 μm diameter range, while in the track, plume particles are preferentially activated into the > 7 μm size range because of their higher number concentration, and the optical depth of continental aerosols falls from 12.38 to 4.44. Continental and plume particles in the 1–7 μm size category also contribute to the track optical depth, which reduces the cloud average effective radius from 5.8 to 4.1 μm.

As with the clean marine cloud, the increase in number density and decrease in effective radius combines to increase the track optical depth, and there is an additional contribution from the LWC, which increases from 0.21 g m^{-3} in the ambient cloud to 0.22 g m^{-3} (a ~5% increase) in the ship track. Also, as with the clean marine cloud, particles with diameter < 1 μm contribute $< 1\%$ to the total optical depth.

Table 4 shows the predicted albedo, absorption, and transmission of the continentally influenced cloud and ship track. Here the albedo is defined at solar zenith

Table 4. Predicted Albedo, Absorption, and Transmission of the Continentally Influenced Ambient Cloud and Track for 55% Updraft/45% Downdraft, 0% Dilution, and Dust Supermicron Particle Composition

	Ambient Cloud, JDT178a		Track, JDT178t	
	All Species	Pure Water	All Species	Pure Water
Albedo	0.556	0.565	0.642	0.666
Absorption, W m^{-2}	65.1	41.5	96.9	41.5
Transmission	0.389	0.404	0.264	0.295

Notation is the same as in Table 2, except that the solar zenith angle is 25.4°.

angle 25.4°. The increase in total optical depth from the continentally influenced ambient cloud to the ship track translates into a smaller yet significant increase in predicted albedo (15%), from 0.556 to 0.642; the already somewhat polluted marine cloud is less susceptible to the reflectivity increase imposed by the ship track than is the clean marine cloud (cf. to results of *Durkee et al.* [2000b]). However, the continentally influenced cloud absorbs nearly twice the amount of the clean marine cloud, 65.1 W m^{-2} in the ambient cloud and 96.9 W m^{-2} in the ship track, because of its high absorbing aerosol content. (See section 5.) This amount of absorption is higher than what is predicted by most radiative transfer models but is comparable to the maximum value of 150 W m^{-2} reported by *Cess et al.* [1995] and *Ramanathan et al.* [1995]. The increase in reflectivity and absorption from the ambient cloud to the ship track decreases the transmission of the continentally influenced cloud from 0.389 to 0.264.

The radiative properties for a pure water cloud with the same size distribution as the continentally influenced marine cloud are also shown in Table 4. In contrast to the clean marine cloud, in both the ambient cloud and ship track, there is a significant difference in radiative properties between the pure water cloud and the all-species cloud. The pure water cloud absorbs 36–57% less than the all-species cloud, and has a 2–4% higher albedo and a 11–31% higher transmission. This agrees with the analysis of *Bazhenov et al.* [1994], who found that the incorporation of haze particles in droplet structure can increase visible light absorption by 2 orders of magnitude. As with the clean marine stratocumulus, the radiative properties of the continentally influenced marine stratocumulus are dominated by activated droplets. However, in the continentally influenced case, the droplets contain enough absorbing components to significantly affect the magnitude of their absorption and transmission. (See section 5 for further analysis.)

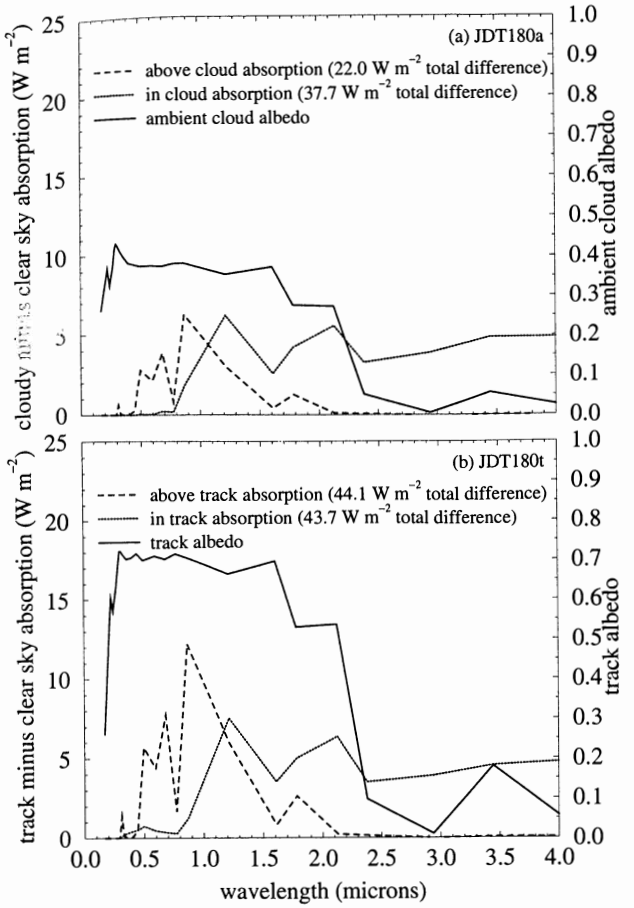

Figure 3. (a) Difference in above- and in-cloud absorption between the clean marine ambient cloud (JDT180a) and a clear sky, with cloud albedo superimposed; (b) difference in above- and in-cloud absorption between the clean marine track (JDT180t) and a clear sky, with track albedo superimposed. In both plots the clear sky contains neither clouds nor aerosols and the relative humidity profile does not change between the cloudy sky (or track) and the clear sky. The relative humidity in the track varies slightly from that in the cloud.

5. Absorption Characteristics and the Unexplained Solar Cloud Forcing Issue

5.1. Wavelength Dependent Absorption

To further investigate which species are responsible for the absorption characteristics of each cloud and ship track, in Figures 3 and 4, we plot the above-cloud and in-cloud absorption as a function of wavelength. These plots are again created from our base case model results, with updraft velocity 0.3 m s^{-1}, 55% updraft/45% downdraft, "mixed composition" downdraft mixing rule (see section 6.2), 0% dilution (see section 6.3), dust in supermicron continental particles, solar constant 1358 W m^{-2}, and solar zenith angle 25.4°-25.5°. The absorption is plotted as a difference between absorption in the cloudy atmosphere and absorption in a cloud-free atmosphere $(A_{\text{cloudy}} - A_{\text{clear}})(\lambda)$, where the temperature and vapor profiles remain constant from the cloud to the no-cloud scenarios both outside and within the cloud layers. This is to ensure that the difference in absorption is due only to the presence of the cloud drops and not to a change in vapor profile (which would only serve to enhance the effect). In Figure 3a, corresponding to the clean marine ambient cloud, the peaks in above-cloud absorption occur mostly below 2.0 μm wavelength, where there is strong absorption by water vapor and O_3 and moderately high cloud albedo. These peaks indicate that the principal source of the extra above-cloud absorption is the interaction between scattering off of the cloud top and absorption by water vapor and O_3 above the cloud. *Ramaswamy and Freidenreich* [1998] and *Harshvardhan et al.* [1998] also found an enhancement of vapor absorption above low clouds, specifically in the weaker vapor bands in the near infrared.

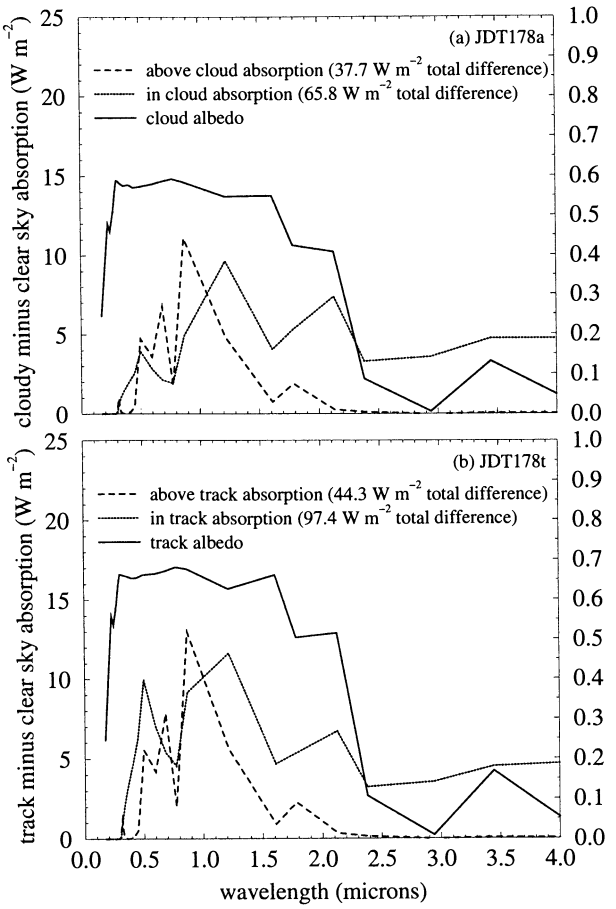

Figure 4. (a) Difference in above- and in-cloud absorption between the continentally influenced ambient cloud (JDT178a) and a clear sky, with cloud albedo superimposed; (b) difference in above- and in-cloud absorption between the continentally influenced track (JDT178t) and a clear sky, with track albedo superimposed. In both plots the clear sky contains neither clouds nor aerosols and the relative humidity profile does not change between the cloudy sky (or track) and the clear sky. The relative humidity in the track varies slightly from that in the cloud.

In contrast, the peaks in in-cloud absorption occur at wavelengths > 0.7 μm, where there is strong absorption by water vapor and liquid water [*Ramaswamy and Freidenreich*, 1998]. This indicates that the source of the extra in-cloud absorption is the interaction between scattering by the cloud drops and absorption by water vapor and by the cloud drops themselves. The fact that there is extra in-cloud absorption may be a factor in the atmospheric absorption enhancements found in cloudy atmospheres by *Cess and Zhang* [1996], *Pilewski and Valero* [1996], *Ramaswamy and Freidenreich* [1998], and *Harshvardhan et al.* [1998], who found that absorption by a cloud can occur in addition to, as well as in place of, clear-sky absorption. It also agrees with the analysis of *King et al.* [1993], who attributed the increase in near infrared absorption in ship tracks to absorption by liquid water. Furthermore, the total amount of extra in-cloud absorption, 50.8 W m^{-2}, may be compared with the 56 W m^{-2} residual absorption found by *Kondratyev et al.* [1995] over the Azov Sea.

Figure 3b, corresponding to the clean marine track, shows a very similar spectral dependence to the clean marine ambient cloud in both the above-track absorption and the in-track absorption. The magnitude of the absorption, however, is greater in the wavelength region below 2.0 μm, where the track albedo is greater. Here the higher track optical depth (note that the LWC for the cloud considered in Figure 3b is ~5% more than that in Figure 3a) and higher albedo cause more scattering, increase the path length of the radiation above and within the cloud, and increase the opportunity for the radiation to be absorbed. The microphysical influences due to the ship track plume cause an increase in the above-cloud absorption of 22 W m^{-2} while the in-cloud absorption increases by 6 W m^{-2}, yielding an atmospheric absorption enhancement of 28 W m^{-2}. Note that the clear-sky temperature and vapor profiles in the track influenced atmosphere vary slightly from the clear-sky profiles in the ambient cloud influenced atmosphere. (The clear-sky track layer profiles match those of the cloudy sky track rather than those of the clear-sky ambient cloud.) However, this variation has a negligible effect on the results, and therefore the difference in spectral dependence between Figure 3a and Figure 3b reflects almost exclusively the effect of pollution on cloud albedo and atmospheric absorption enhancement. The same is true for Figures 4a and 4b.

In Figure 4a, corresponding to the continentally influenced ambient cloud, the peaks in above-cloud absorption again occur mostly below 2.0 μm wavelength, where there is strong absorption by water vapor and O_3, and a high cloud albedo. Again these peaks indicate that the source of the extra above-cloud absorption is the interaction between scattering off of the cloud top and absorption by water vapor and O_3 above the cloud. The in-cloud absorption, however, has a new peak around 0.5 μm wavelength, where both dust and carbonaceous species absorb strongly. Here the dust and organic carbon in the activated continental aerosol particles not only increase the magnitude of the in-cloud absorption but also alter its wavelength dependence. The total amount of extra in-cloud absorption, 65.8 W m^{-2}, is within the range of residual absorption (21–77 W m^{-2}) measured by *Kondratyev et al.* [1995] in polluted environments for clouds of optical thickness 16–38.

Figure 4b, corresponding to the continentally influenced track, shows a very similar spectral dependence to the continentally influenced ambient cloud in both the above-track absorption and the in-track absorption. However, as in the clean marine case, the magnitude of the absorption in the track is greater in the wavelength region below 2.0 μm than in the ambient cloud. The track optical depth and albedo are not only higher in this region, creating a larger path length for the radia-

tion, but the track also contains a significantly higher content of carbonaceous species than the ambient cloud. Both the dust in the activated continental aerosols and the organic and black carbon in the activated plume aerosols increase the magnitude of the track absorption at 0.5 μm wavelength. Compared to the clean marine cloud case, the ship track plume influence on the microphysics causes an atmospheric absorption enhancement of 37 W m^{-2}. However, this enhancement is dominated more by the in-cloud absorption (31 W m^{-2}) rather than the above-cloud absorption (6 W m^{-2}). Thus the type of air mass governs the net influence of the ship track plumes, including whether it is the above- or in-cloud absorption that is more affected.

5.2. Applications to the Solar Forcing Puzzle

Beginning with *Cess et al.* [1995], *Ramanathan et al.* [1995], and *Pilewski and Valero* [1995], there have been a number of recent articles addressing whether clouds absorb more solar radiation than is predicted by radiative transfer models. *Cess et al.* [1995], *Ramanathan et al.* [1995], and *Pilewski and Valero* [1995] derived a solar cloud-forcing ratio from their measurements, invariant with respect to season and location, of 1.5, whereas current GCMs generally produce a ratio closer to 1.0 [*Cess et al.*, 1995]. Here cloud-forcing is defined as

$$C_s = (F^{\downarrow}_{\text{cloudy}} - F^{\uparrow}_{\text{cloudy}}) - (F^{\downarrow}_{\text{clear}} - F^{\uparrow}_{\text{clear}}), \quad (2)$$

and the cloud-forcing ratio is

$$R = \frac{C_s(S)}{C_s(\text{TOA})}, \quad (3)$$

where $F^{\uparrow}$ and $F^{\downarrow}$ are the upward and downward total solar irradiances, S represents the surface, and TOA represents the top of the atmosphere. *Collins* [1998] has also determined that enhanced shortwave absorption occurs with minimal seasonal and interannual variability. *Kondratyev et al.* [1995], *Li et al.* [1995], *Li and Moreau* [1996], and *Harshvardhan et al.* [1998], however, have shown that R can be highly variable and that large values of R may be associated with heavy pollution.

In Table 5 we show the cloud-forcing ratios calculated from our base case clean and continentally influenced marine cloud distributions and their associated ship track effects. For the clean marine cloud, our R values of 1.20 and 1.15 may be compared with the values reported by *Kondratyev et al.* [1995] for clean environments (1.07–1.16) and with the typical range of values reported by *Li and Moreau* [1996] for midlatitude regions (1.0–1.2). They also fall within the values of 1.14 and 1.31 (for wavelengths > 0.55 μm) calculated by *Harshvardhan et al.* [1998] for low clouds.

For the continentally influenced marine cloud, we have two sets of calculations, depending on the composition of the supermicron continental particles, which was not determined. (See section 6.4.) Assuming that they are composed of mineral dust, the cloud-forcing ratios are 1.22 and 1.26 for the ambient cloud and track, respectively. If they are composed instead of black carbon, the cloud-forcing ratios increase to 1.37 and 1.27, respectively. These values are much lower than the value reported by *Kondratyev et al.* [1995] for a polluted environment (2.6) and generally smaller than the range of values reported by *Evans et al.* [1995] (1.4–2.0) but are greater than that produced by the model of *Li and Moreau* [1996], which rarely produces a ratio larger than 1.25. The above are merely illustrative examples calculated at a particular solar zenith angle. We have not examined the diurnal-mean estimates, but rather are proposing a mechanism that could potentially yield higher values of cloud-forcing ratio through aerosol-cloud microphysical interactions.

Note that the cloud-forcing ratio actually decreases from the marine ambient cloud to its associated ship track, which might not be intuitively expected. Although there is more absorption in the ship track, because of the manner in which the cloud forcing ratio is defined in terms of TOA and surface irradiances the increase in optical depth in the ship track can actually result in a decrease in cloud-forcing ratio. Note also that the clear sky as defined in these calculations does not include aerosols. The inclusion of aerosols in the clear sky may decrease the cloud-forcing ratio, particularly in the continentally influenced case. However, the

Table 5. Ratio of Modeled Total Solar Cloud-Forcing at the Surface to Modeled Total Solar Cloud-Forcing at the Top of the Atmosphere

Case	C_s(S)/C_s(TOA)
Clean marine ambient cloud, JDT180a	1.20
Clean marine track, JDT180t	1.15
Continentally influenced ambient cloud, JDT178a	
Dust supermicron continental particle composition	1.22
Black carbon supermicron continental particle composition	1.37
Continentally influenced track, JDT178t	
Dust supermicron continental paricle composition	1.26
Black carbon supermicron continental particle composition	1.27

Table 6. Sensitivity of Model Results for the Clean Marine Cloud With Respect to the Base Case of (1) Updraft Velocity 0.3 m s^{-1}, (2) 55% Updraft/45% Downdraft, (3) "Mixed Composition" Downdraft Mixing Rule, and (4) 0% Dilution

	N_d, cm^{-3}	r_{eff}, μm	LWC, g m^{-3}	τ_{ext}	Albedo
Clean Marine Ambient Cloud, JDT180a					
Updraft velocity					
0.2 m s^{-1}	53	10.6	0.18	6.19	0.323
0.3 m s^{-1}	53	10.8	0.19	7.17	0.361
0.5 m s^{-1}	54	10.9	0.21	6.90	0.353
Updraft/downdraft					
45%/55%, mixed composition	43	10.8	0.15	5.88	0.318
45%/55%, mixed fluxes	43	10.8	0.15	5.88	0.250
55%/45%, mixed composition	53	10.8	0.19	7.17	0.361
55%/45%, mixed fluxes	53	10.8	0.19	7.17	0.265
65%/35%, mixed composition	62	10.8	0.22	8.46	0.398
65%/35%, mixed fluxes	62	10.8	0.22	8.46	0.301
100%/0%	96	10.8	0.34	12.98	0.496
Clean Marine Track, JDT180t					
Updraft velocity					
0.2 m s^{-1}	2610	3.7	0.18	17.18	0.617
0.3 m s^{-1}	2130	3.4	0.20	22.89	0.673
0.5 m s^{-1}	2720	2.8	0.23	30.05	0.727
Updraft/downdraft					
45%/55%, mixed composition	1750	3.4	0.16	18.75	0.635
45%/55%, mixed fluxes	1750	3.4	0.16	18.75	0.380
55%/45%, mixed composition	2130	3.4	0.20	22.89	0.673
55%/45%, mixed fluxes	2130	3.4	0.20	22.89	0.452
65%/35%, mixed composition	2520	3.4	0.23	27.05	0.701
65%/35%, mixed fluxes	2520	3.4	0.23	27.05	0.522
100%/0%	3880	3.4	0.36	41.56	0.763
Dilution					
0%	2130	3.4	0.20	22.89	0.673
50%	2200	3.0	0.20	19.63	0.679
90%	336	5.7	0.20	14.65	0.554

Here N_d is cloud drop number concentration; r_{eff} is effective radius; LWC is cloud liquid water content; τ_{ext} is 0.55 μm cloud extinction optical depth; Albedo is simulated MRF C-130 broadband radiometer albedo, defined at altitude 1000 m, solar zenith angle 25.5°, and wavelength 0.3–3.0 μm; mixed composition is the mixed composition mixing rule; mixed fluxes are the mixed radiative fluxes mixing rule.

inclusion of aerosols in the clear sky is dependent on a somewhat arbitrary choice of relative humidity within the layer in which clouds were present in the "cloudy" sky case. Because of this ambuigity, we leave the topic of the definition of clear sky as the subject of a separate study and choose to focus here on the forcing by the cloud and aerosol system with respect to a cloud- and aerosol-free sky.

Our results lead us to conclude, in agreement with *Kondratyev et al.* [1995] and *Li and Moreau* [1996], that the solar cloud-forcing ratio is highly variable and that absorbing aerosol particles incorporated into cloud drops could go a long way toward reconciling possible gaps between theoretical treatments and measured estimates of solar absorption in cloudy atmospheres. The aerosol-induced cloud modifications can be expected to be region- and airflow-dependent. They comprise a component that is sensitive to the enhanced reflection by cloud and subsequent increase caused by gaseous absorption above, an effect which would be further exacerbated if the water vapor profile in cloudy skies differs from that in the clear ones.

6. Sensitivity Studies

Tables 6 and 7 show the sensitivity of our model results to uncertainties in the model input parameters. All runs are variations from our base case (updraft velocity w = 0.3 m s^{-1}, 55% updraft/45% downdraft, "mixed composition" downdraft mixing rule, 0% dilution, and dust in supermicron continental particles).

6.1. Updraft Velocity

As the updraft velocity increases, the maximum supersaturation attained also increases. However, depending on the number of efficient cloud condensation

Table 7. Sensitivity of Model Results for the Continentally Influenced Cloud With Respect to the Base Case of (1) Updraft Velocity 0.3 m s^{-1}, (2) 55% Updraft/45% Downdraft, (3) "Mixed Composition" Downdraft Mixing Rule, (4) 0% Dilution, and (5) Dust Supermicron Continental Particle Composition

	N_d, cm^{-3}	r_{eff}, μm	LWC, g m^{-3}	τ_{ext}	Albedo
Continentally Influenced Ambient Cloud, JDT178a					
Updraft velocity					
0.2 m s^{-1}	333	5.6	0.19	14.49	0.546
0.3 m s^{-1}	301	5.8	0.21	14.67	0.556
0.5 m s^{-1}	351	5.6	0.25	15.00	0.561
Updraft/downdraft					
45%/55%, mixed composition	246	5.8	0.17	12.05	0.512
45%/55%, mixed fluxes	246	5.8	0.17	12.05	0.339
55%/45%, mixed composition	301	5.8	0.21	14.67	0.556
55%/45%, mixed fluxes	301	5.8	0.21	14.67	0.401
65%/35%, mixed composition	356	5.8	0.25	17.26	0.591
65%/35%, mixed fluxes	356	5.8	0.25	17.26	0.462
100%/0%	547	5.8	0.39	26.39	0.671
Supermicron composition					
Dust	301	5.8	0.21	14.67	0.556
Black carbon	301	5.8	0.21	14.67	0.530
Continentally Influenced Track, JDT178t					
Updraft velocity					
0.2 m s^{-1}	902	4.5	0.19	18.99	0.604
0.3 m s^{-1}	985	4.1	0.22	22.10	0.642
0.5 m s^{-1}	963	3.7	0.25	22.33	0.641
Updraft/downdraft					
45%/55%, mixed composition	806	4.1	0.18	18.23	0.606
45%/55%, mixed fluxes	806	4.1	0.18	18.23	0.378
55%/45%, mixed composition	985	4.1	0.22	22.10	0.642
55%/45%, mixed fluxes	985	4.1	0.22	22.10	0.443
65%/35%, mixed composition	1160	4.1	0.25	25.98	0.669
65%/35%, mixed fluxes	1160	4.1	0.25	25.98	0.507
100%/0%	1790	4.1	0.39	39.55	0.727
Dilution					
0%	985	4.1	0.22	22.10	0.642
50%	594	5.2	0.21	18.27	0.603
90%	356	5.7	0.21	14.98	0.556
Supermicron composition					
Dust	985	4.1	0.22	22.10	0.642
Black carbon	985	4.1	0.22	22.10	0.639

Notation is the same as in Table 5, except that the albedo is defined at solar zenith angle 25.4°; supermicron composition is supermicron continental particle composition.

nuclei, the cloud drop number (N_d), optical depth, and albedo may or may not increase in response [*Russell et al.*, 1999]. To investigate the influence of this effect on our results, we vary the updraft velocity in each of our cases from 0.2 to 0.5 m s^{-1}.

In the clean marine ambient cloud, there is very little difference in N_d or LWC as the updraft velocity varies from 0.2 to 0.5 m s^{-1}. However, the w = 0.2 m s^{-1} and w = 0.5 m s^{-1} runs have a lower optical depth (τ_{ext}) and albedo than the base case (w = 0.3 m s^{-1}). This is due to the fact that the w = 0.2 m s^{-1} run has a lower LWC, while the w = 0.5 m s^{-1} run has a higher effective radius (r_{eff}). As w varies, τ_{ext} varies between 6.19 and 7.17, and the albedo varies between 0.323 and 0.361. Note that the concept of an r_{eff} is a rather coarse description of the finer grain changes that occur in the size spectrum as revealed by the explicit modeling results shown in Figures 1 and 2.

In the clean marine track, a higher number of cloud drops are activated for w = 0.2 m s^{-1} and w = 0.5 m s^{-1} than for w = 0.3 m s^{-1}. This is due to the fact that the w = 0.2 m s^{-1} run has a lower maximum supersaturation than the base case but a longer time available for particles to grow by condensation. The w = 0.5 m s^{-1} run, however, has a higher maximum supersaturation than the base case. Despite the higher N_d for w = 0.2 m s^{-1} and w = 0.5 m s^{-1}, the LWC, τ_{ext}, and albedo increase monotonically as w increases. As w increases, τ_{ext} increases from 17.18 to 30.05, and the albedo increases from 0.617 to 0.727.

The same is true for the continentally influenced ambient cloud (Table 7), where both $w = 0.2$ m s^{-1} and $w = 0.5$ m s^{-1} have higher cloud drop numbers than the base case, but because the LWC increases with w, so do τ_{ext} and the albedo. For the continentally influenced ambient cloud, as w increases, τ_{ext} increases from 14.49 to 15.00, and the albedo increases from 0.546 to 0.561.

In the continentally influenced track, a lower number of cloud drops is activated for $w = 0.2$ m s^{-1} and $w = 0.5$ m s^{-1} than for $w = 0.3$ m s^{-1}. This is due to the fact that the $w = 0.2$ m s^{-1} run has a lower maximum supersaturation than the base case. Although the $w = 0.5$ m s^{-1} run attains a higher maximum supersaturation than the base case, it does not provide enough time for particles to grow, as evidenced by the lower r_{eff}. In the continentally influenced track, both the LWC and τ_{ext} increase monotonically as w increases from 0.2 m s^{-1} to 0.5 m s^{-1}. The albedo likewise increases from $w = 0.2$ m s^{-1} to $w = 0.3$ m s^{-1}, but because the $w = 0.5$ m s^{-1} run has a lower N_d than the $w = 0.3$ m s^{-1} run, the albedo is slightly lower for $w = 0.5$ m s^{-1} than for $w = 0.3$ m s^{-1}. As w increases, τ_{ext} increases from 18.99 to 22.33, and the albedo varies between 0.604 and 0.642. A key point emerging is that there can be nonmonotonic changes in r_{eff} and N_d with updraft, depending on the initial size spectrum and the type of air mass in question; this, in turn, affects the optical depth and albedo in an appropriate manner.

6.2. Updraft/Downdraft Fraction

Updraft regions of clouds tend to have a higher droplet concentration, LWC, and τ_{ext} than downdraft regions, which contain evaporating and subsaturated droplets (see Tables 1 and 3). Therefore uncertainty in the updraft area fraction can lead to uncertainty in the average τ_{ext} and albedo for the cloud as a whole. To take this effect into account, we have varied the updraft area fraction in our model within accepted limits based on observations [*Brooks and Rogers*, 1997; D. Johnson, personal communication, 1999] and large eddy simulations [*Stevens et al.*, 1998; B. Stevens, personal communication, 1999].

In order to vary the updraft region of the cloud, we use two separate mixing rules. In the first, labeled "mixed composition," we linearly combine the τ_{ext}, single-scattering albedo, and asymmetry factor of the updraft and downdraft regions in each layer. In the second, labeled "mixed fluxes," we run the updrafts and downdrafts separately through the radiative transfer code. Then we linearly combine the upward and downward irradiances at the cloud boundaries. Because of the nonlinear nature of the problem, the "mixed flux" albedos tend to be unrealistically low, while the "mixed composition" runs (our base cases) tend to approximate the mixing more reasonably.

In all cases, the maximum supersaturation and effective radius of the droplets remain essentially unchanged as the updraft area fraction increases from 45 to 100%. The cloud drop number and LWC, however, vary almost linearly with updraft area fraction, and the optical depth and albedo increase correspondingly. As the updraft area fraction increases from 45 to 65%, using the mixed composition mixing rule τ_{ext} increases by 43–44% and the albedo increases by 10–25%. Overall, the behavior is a linear, monotonic one in contrast to that for the updraft speed considerations.

6.3. Dilution

While we use 0% dilution as our base case, ship plume emissions tend to dilute with track age and distance from the track head [*Hobbs et al.*, 2000; *Durkee et al.*, 2000a], thus decreasing the track albedo. To simulate this effect, we dilute the ship plume particle and SO_2 emissions by 50 and 90% for both of our ship tracks. With 50 and 90% dilution, the maximum supersaturation and LWC remain largely unchanged. However, the cloud drop numbers decrease substantially.

In the clean marine track, as dilution switches from 0 to 90%, N_d decreases from 2130 to 336 cm^{-3}, r_{eff} increases from 3.4 to 5.7 μm, τ_{ext} decreases from 22.89 to 14.65, and the albedo decreases from 0.673 to 0.554. The 50% dilution run, however, has the highest N_d and the lowest r_{eff}. The explanation for this lies in the saturation of the activation process. At 0% dilution, the activation process is saturated because of the high particle number, and the resulting cloud contains a large number of haze particles. At 50% dilution, some of these haze particles move into the small droplet regime, thereby increasing the cloud drop number and shifting the effective radius of activated drops toward smaller droplets. The increase in N_d and decrease in r_{eff} also give the 50% dilution run the highest albedo, 0.679. In the continentally influenced track, as dilution increases, N_d decreases from 985 to 356 cm^{-3}, r_{eff} increases from 4.1 to 5.7 μm, τ_{ext} decreases from 22.10 to 14.98, and the albedo decreases accordingly from 0.642 to 0.556. Again, a nonmonotonic variation is seen to occur depending on the initial conditions and the aerosol size distribution in question.

6.4. Composition of Supermicron Continental Particles

Although the size distribution of continental particles is determined from the measured background distributions of clean marine case and the continentally influenced case (refer to section 3), there is some uncertainty in their composition. Specifically, a small number ($\sim$5 cm^{-3}) of supermicron continental particles exist, which are not expected to be plume, marine sulfate, or sea salt at the measured wind speeds. Because of their large size, these supermicron particles have the potential to strongly influence the absorption characteristics of the continentally influenced cloud. As our base case, we assign the largest fraction of the supermicron continental particle mass to mineral dust (mod-

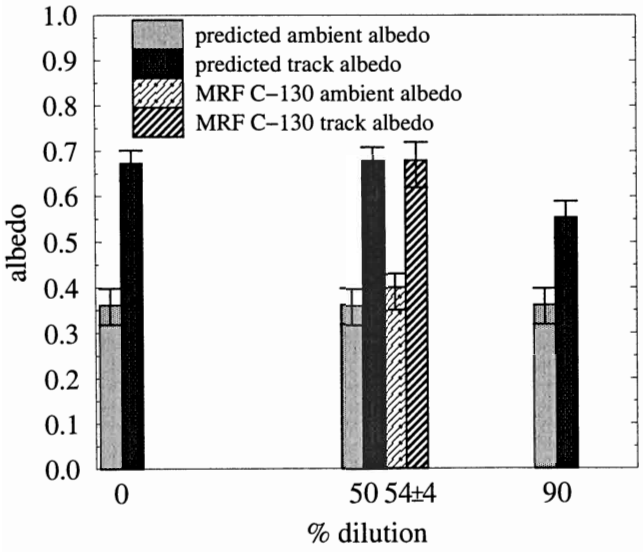

Figure 5. Comparison to albedo measurements for the clean marine stratocumulus (JDT180) as a function of track dilution. The error bars on the predicted albedos represent the change in albedo as the updraft area fraction increases from 45 to 65%; the error bars on the measured values represent the noise in the meaurements and the differences in magnitudes between multiple peaks during the time section (June 29, 1994, Greenwich Mean Time (GMT) 18:48:40–18:53:40).

erately absorbing). However, to test the sensitivity of this assumption we also show results where the dust has been switched to black carbon (strongly absorbing). In both the continentally influenced ambient cloud and ship track, the optical depth remains largely unchanged when the supermicron continental particle composition is changed to black carbon. However, the albedo decreases significantly in response to the increasing absorption, from 0.556 to 0.530 in the continentally influenced ambient cloud and from 0.642 to 0.639 in the continentally influenced track. As discussed in section 5.2, the influence of supermicron continental particle composition on cloud absorption is also evident in the solar cloud-forcing ratios in Table 5. For both the continentally influenced ambient cloud and continentally influenced track, the solar cloud-forcing ratio is greater for supermicron particles consisting of black carbon than for supermicron particles consisting of mineral dust.

7. Comparison With Measured Albedos

In Figures 5 and 6, we compare our model results against MRF C-130 radiometer measurements, in the wavelength region 0.3–3.0 μm. For each calculated albedo, the altitude at which the albedo is calculated (1000 m) and the solar zenith angle in the model (25.4°–25.5°) are set to match the elevation and time of day of the MRF C-130 measurements. The albedo is presented as a function of track dilution (see section 6.3), where 0% dilution represents conditions at the track head, and the higher dilutions represent conditions farther down the track and as the track aged, where both the ship plume particle concentration and the SO_2 emissions are reduced. For each calculation, there is a pair of mean albedos depicted as vertical rectangular bars, the lower one for the ambient cloud and the higher one for the ship track. The vertically drawn delimiters on each of the rectangular bars of the modeled albedos represent the change in albedo as the updraft fraction varies from 45 to 65% (see section 6.2).

Analysis of the MRF C-130 measurements is complicated by the fact that they were not collocated with the UW C-131A aerosol measurements used to initialize our model (see section 3). The MRF measurements were in fact of the order of 3 hours apart from the aerosol measurements. Furthermore, the MRF C-130 did not sample the track made by the ship *Star Livorno* (our clean marine case) but did sample a neighboring track made by the ship *Hanjin Barcelona* under similar conditions. The thicknesses of the clouds are quite similar, but there is a shift in cloud height between the UW and the MRF measurements and a corresponding change in temperature profile, which could by itself cause some discrepancy between predictions and observations. In an attempt notwithstanding these problems, we plot the MRF C-130 meaurements along side our model results, where the pair of albedos again represent the ambient cloud and ship track, respectively. The vertical delimiters drawn on the rectangular bars for the mean measured albedos represent the noise in the pyranometer signal and the variation in the magnitude of the albedo

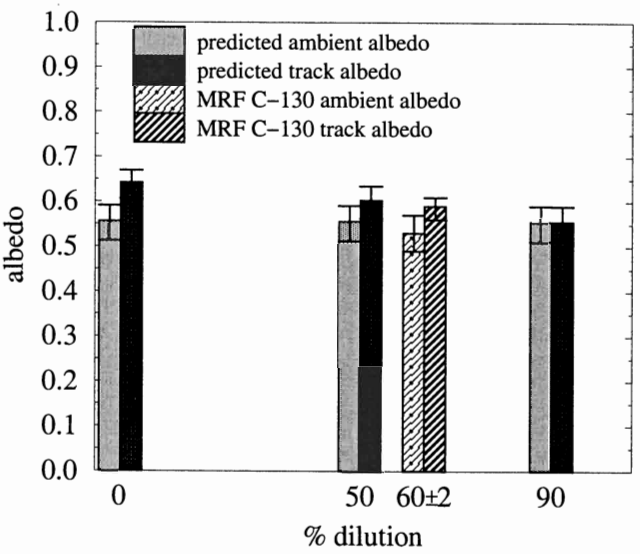

Figure 6. Comparison to albedo measurements for the continentally influenced marine stratocumulus (JDT178) as a function of track dilution. The error bars on the predicted albedos represent the change in albedo as the updraft area fraction increases from 45 to 65%; the error bars on the measured values represent the noise in the meaurements and the differences in magnitudes between multiple peaks during the time section (June 27, 1994, GMT 18:29:13–18:40:56).

when more than one ship track induced peak appeared in the same time series section.

The dilution of the MRF albedos is calculated with the aid of advanced very high resolution radiometer (AVHRR) analysis of track width versus track age for the *Star Livorno* and *Tai He*, respectively [*Durkee et al.*, 2000a], where the AVHRR images used are chosen closest to the UW C-131A measurements. The track ages at the time and location where the MRF C-130 intercepted the *Hanjin Barcelona* and the *Tai He* are determined through advection analysis (K. Nielsen, personal communication, 1999). Then, assuming that during the MRF C-130 measurements the tracks had the same widths as similarly aged track segments in the AVHRR measurements, the widths of the tracks during the MRF C-130 measurements are determined through a linear regression of track width versus track age. Given the width w of each track during the MRF C-130 measurements, the dilution is then determined from *Hobbs et al.* [2000, equation (3)], where the average concentration $\overline{X}$ of an effluent is inversely proportional to the track width, $\overline{X} \propto 1/\mathrm{w}$. Therefore

$$\text{dilution} = 1 - \frac{\overline{X}}{\overline{X_0}} = 1 - \frac{\mathrm{w}_0}{\mathrm{w}}, \tag{4}$$

where w_0 is the width at track head. Errors in the regression of track width versus track age and uncertainty in the advection analysis of the track ages during the MRF C-130 measurements are propagated to determine the uncertainty in the calculated dilution for the measurements. This uncertainty is indicated on the x axes of Figures 5 and 6.

In Figures 5 and 6, there is a reasonable agreement between the predicted albedos and the MRF C-130 measurements, both in the ambient clouds and in the ship tracks. In the clean marine case, although the measured ambient cloud and track albedos are slightly higher than the modeled ambient cloud and track albedos, respectively, they are in fair agreement considering the uncertainty in both the measured and modeled values. In the continentally influenced case, the MRF C-130 track albedo fits the model curve of track albedo versus dilution considering the uncertainty limits estimated, with a value lying in between the modeled value at 50% dilution and the modeled value at 90% dilution. Despite the difficulties inherent in the comparison, the model is able to mimic the increase in albedo from the ambient cloud to the ship track rather well in comparison with aircraft radiometer measurements during the MAST campaign.

AVHRR ambient cloud and track albedos as a function of distance from track head were also tabulated during the MAST experiment [*Durkee et al.*, 2000a]. However, the AVHRR albedo measurements do not lend themselves as well to this type of comparison with model results. Because the AVHRR instrument measures the albedo remotely and over a much larger scale (1.1 km spatial resolution), in order to determine the albedo of a particular cloud and ship track, a pixel-by-pixel analysis must be performed, in which it must be determined which pixels are "ambient cloud" and which are "track" (K. Nielsen, personal communication, 1999). Such analysis has to account for inhomogeneities within a single pixel (mixing of ambient cloud with track or mixing of clear sky with cloud), details of which are unquantified. The results of pixel-by-pixel analysis of individual tracks, in fact, tend to be quite noisy (K. Nielsen, personal communication, 1999), and such analysis lends itself better to a larger sample of clouds [e.g., *Durkee et al.*, 2000a]. This subject is beyond the scope of the present study.

Pixel-by-pixel analysis of the *Star Livorno* and *Tai He* tracks from AVHRR images results in almost zero difference between the ambient cloud and track albedos within the uncertainty due to noise in the results (K. Nielsen, personal communication, 1999). This is in sharp contrast to our results and to the in situ MRF C-130 albedo measurements, where there are significant differences between the ambient cloud and track albedos. In addition, the track albedos derived from channel 1 of the AVHRR instrument (0.63 μm) for the *Star Livorno* are of the order of 50% lower than our calculations and the MRF meaurements, hovering around 0.350. Likewise the ambient cloud and track albedos derived from AVHRR channel 1 for the *Tai He* are of the order of 20% lower than our calculations and the MRF measurements, hovering around 0.450 and 0.500, respectively. Because of the poor agreement with the MRF measurements and high amount of noise in the data, we do not undertake comparison with AVHRR-derived albedos here. This requires a separate intensive study to be done in the future.

8. Comparison With Parameterizations

Tables 8 to 11 compare our results against the parameterizations of *Twomey et al.* [1984], *Jones et al.* [1994], and *Feichter et al.* [1997]. To mimic *Twomey et al.* [1984], the scattering optical depths for the ambient clouds, JDT180a and JDT178a, are set to match our effective scattering optical depths, and the scattering optical depths for the ship tracks, JDT180t and JDT178t, are calculated assuming no change in LWC, such that

$$\tau_{\mathrm{sca}_{\mathrm{track}}} = \tau_{\mathrm{sca}_{\mathrm{ambient}}} \left(\frac{N_{d_{\mathrm{track}}}}{N_{d_{\mathrm{ambient}}}} \right)^{1/3}, \tag{5}$$

where $\tau_{\mathrm{sca}_{\mathrm{track}}}$ and $\tau_{\mathrm{sca}_{\mathrm{ambient}}}$ are the track and ambient cloud scattering coefficients and $N_{d_{\mathrm{track}}}$ and $N_{d_{\mathrm{ambient}}}$ are the track and ambient cloud drop concentrations, respectively. The absorption coefficients are calculated from *Twomey et al.* [1984] using

$$\beta_{\mathrm{abs}} = 10^{-5} N_d^{2/3}, \tag{6}$$

where β_{abs} is the absorption coefficient in km^{-1} and N_d

Table 8. Comparison With Parameterizations for the Clean Marine Ambient Cloud (JDT180a)

Parameter	*Twomey et al.* [1984]	*Jones et al.* [1994][a]		*Feichter et al.* [1997][b]		This Study
		N_d Calc	N_d Given	N_d Calc	N_d Given	
N_a, cm^{-3}	n.a.[c]	104	n.a.	n.a.	n.a.	104
$m_{SO_4^{2-}}$, μg m^{-3}	n.a.	n.a.	n.a.	1.3	n.a.	1.3
m_{OC}, μg m^{-3}	n.a.	n.a.	n.a.	n.a.	n.a.	0
m_{BC}, μg m^{-3}	n.a.	n.a.	n.a.	n.a.	n.a.	0
N_d, cm^{-3}	53	86	53	130	53	53
LWC, g m^{-3}	n.a.	0.19	0.19	0.19	0.19	0.19
Δz, m	220	220	220	220	220	220
Type	n.a.	M	M	M	M	M
r_{eff}, μm	n.a.	8.7	10.2	7.7	10.4	10.8
τ_{sca}	7.17	n.a.	n.a.	n.a.	n.a.	7.17
β_{abs}, km^{-1}	1×10^{-4}	n.a.	n.a.	n.a.	n.a.	2×10^{-5}
τ_{abs}	3×10^{-5}	n.a.	n.a.	n.a.	n.a.	3×10^{-6}
τ_{ext}	7.17	7.43	6.50	8.57	6.20	7.17
ϖ	0.999996	1.000000	1.000000	0.999900	0.999900	0.999999
g	0.86	0.85	0.85	0.86	0.87	0.85
Albedo	0.729	0.405	0.366	0.375	0.297	0.361
Absorption, W m^{-2}	16.8	45.3	45.4	137.8	114.9	39.0
Transmission	0.244	0.568	0.611	0.508	0.613	0.623

Here N_d calc is drop number calculated according to the parameterization, and N_d given is drop number assigned to be equal to this study. N_a is the average precloud aerosol concentration; $m_{SO_4^{2-}}$ is the average precloud submicron sulfate mass; m_{OC} is the average precloud submicron organic carbon mass; m_{BC} is the average precloud submicron black carbon mass; N_d is the cloud average drop number concentration; LWC is the cloud average liquid water content; Δz is the cloud thickness; Type is maritime (M) or continental (C); r_{eff} is the cloud average effective radius; τ_{sca} is the total cloud scattering optical depth at 550 nm; β_{abs} is the cloud average absorption coefficient at 550 nm; τ_{abs} is the total cloud absorption optical depth at 550 nm; τ_{ext} is the total cloud extinction optical depth at 550 nm; ϖ is the cloud average single scattering albedo at 550 nm; g is the cloud average asymmetry factor at 550 nm. The albedo, absorption, and transmission are total 0.30–3.0 μm. All values are base case 55% updraft/45% downdraft, 0% dilution, and solar zenith angle 25.5°.

[a]On the basis of the parameterization of *Slingo* [1989].

[b]On the basis of the parameterization of *Boucher and Lohmann* [1995].

[c]Here n.a., not applicable, i.e., not involved in the parameterization.

is given for each ambient cloud and track, and the asymmetry factor (g) is assigned the representative value of 0.86. The *Twomey et al.* [1984] relationship slightly overestimates β_{abs} in the clean marine ambient cloud and track and underestimates β_{abs} by a couple orders of magnitude in the continentally influenced ambient cloud and track. This, coupled with the fact that the solar radiative transfer is performed effectively assuming a single band in that study, produces a large underestimate of the cloud absorption in all four cases discussed here, and a subsequent overestimate of the cloud albedo and transmission. The *Twomey et al.* [1984] relationship predicts ambient cloud to track albedo increases of only 20% and 5% for the clean and continentally influenced clouds, respectively, whereas our model predicts increases of 86 and 15%.

Jones et al. [1994] and *Feichter et al.* [1997] use empirical formulae to calculate cloud drop number concentration, the former based on the precloud aerosol concentration (N_a), and the latter based on the precloud sulfate mass ($m_{SO_4^{2-}}$). *Jones et al.* [1994] give

$$N_d = 375\left[1 - \exp(-2.5 \times 10^{-3} N_a)\right], \tag{7}$$

while *Feichter et al.* [1997], which is based on *Boucher and Lohmann* [1995], give

$$N_d^{\text{mar}} = 10^{2.24 + 0.257 \log_{10}(m_{SO_4^{2-}})} \tag{8}$$

$$N_d^{\text{cont}} = 10^{2.06 + 0.48 \log_{10}(m_{SO_4^{2-}})}, \tag{9}$$

where $m_{SO_4^{2-}}$ is in μg m^{-3}, mar is maritime, and cont is continental. The results based on these formulae are presented in Tables 8-11 in the columns labeled "N_d calc."

The relationship between N_d and N_a given by *Jones et al.* [1994], derived from a wide collection of observations, is less steep than that produced by our model. *Jones et al.* [1994] tend to yield a larger N_d in the ambient clouds, with values of 86 and 352 cm^{-3}, as compared to our values of 53 and 301 cm^{-3}, respectively. They also tend to yield a lower N_d in the ship tracks, with a value of 375 cm^{-3}, as compared to our values

Table 9. Comparison With Parameterizations for the Clean Marine Track (JDT180t)

Parameter	*Twomey et al.* [1984]	*Jones et al.* [1994]		*Feichter et al.* [1997]		This Study
		N_d Calc	N_d Given	N_d Calc	N_d Given	
N_a, cm^{-3}	n.a.	18,300	n.a.	n.a.	n.a.	18,300
$m_{SO_4^{2-}}$, μg m^{-3}	n.a.	n.a.	n.a.	15.4	n.a.	15.4
m_{OC}, μg m^{-3}	n.a.	n.a.	n.a.	n.a.	n.a.	1.5
m_{BC}, μg m^{-3}	n.a.	n.a.	n.a.	n.a.	n.a.	1.5
N_d, cm^{-3}	2130	375	2130	427	2130	2130
LWC, g m^{-3}	n.a.	0.19	0.19	0.19	0.19	0.20
Δz, m	220	220	220	220	220	220
Type	n.a.	M	M	M	M	M
r_{eff}, μm	n.a.	5.3	3.0	5.2	3.0	3.4
τ_{sca}	24.56	n.a.	n.a.	n.a.	n.a.	22.89
β_{abs}, km^{-1}	2×10^{-3}	n.a.	n.a.	n.a.	n.a.	9×10^{-3}
τ_{abs}	4×10^{-4}	n.a.	n.a.	n.a.	n.a.	3×10^{-3}
τ_{ext}	24.56	11.39	19.39	13.14	23.45	22.89
ϖ	0.999985	1.000000	1.000000	0.999900	0.999900	0.999918
g	0.86	0.84	0.83	0.85	0.84	0.82
Albedo	0.877	0.525	0.653	0.477	0.590	0.673
Albedo increase, %	20	30	78	27	99	86
Absorption, W m^{-2}	17.1	44.4	42.9	170.6	215.0	45.5
Transmission	0.082	0.439	0.301	0.364	0.199	0.277

Notation is the same as in Table 8.

of 2130 and 985 cm^{-3}, respectively. Consequently, they underestimate the effective radius (r_{eff}) in the clean marine ambient cloud and overestimate r_{eff} in the two ship tracks. They also overestimate τ_{ext} in the clean marine ambient cloud and sustantially underestimate τ_{ext} in the two ship tracks.

The N_d parameterization by *Feichter et al.* [1997], based on sulfate mass, underestimates N_d in comparison with our model for all but the clean marine ambient cloud, where their value of 130 cm^{-3} is nearly double our value of 53 cm^{-3}. Consequently their r_{eff} is higher than ours for all but the clean marine ambient cloud, where they predict 7.7 μm as compared to our 10.8 μm. Like *Jones et al.* [1994] they yield a higher τ_{ext} in the clean marine ambient cloud and substantially underestimate τ_{ext} in the two ship tracks.

The differences in the predicted values of N_d are illustrated in Figure 7, where the formulae for computing

Table 10. Comparison With Parameterizations for the Continentally Influenced Ambient Cloud (JDT178a)

Parameter	*Twomey et al.* [1984]	*Jones et al.* [1994]		*Feichter et al.* [1997]		This Study
		N_d Calc	N_d Given	N_d Calc	N_d Given	
N_a, cm^{-3}	n.a.	1110	n.a.	n.a.	n.a.	1110
$m_{SO_4^{2-}}$, μg m^{-3}	n.a.	n.a.	n.a.	5.5	n.a.	5.5
m_{OC}, μg m^{-3}	n.a.	n.a.	n.a.	n.a.	n.a.	0.9
m_{BC}, μg m^{-3}	n.a.	n.a.	n.a.	n.a.	n.a.	0.9
N_d, cm^{-3}	301	352	301	269	301	301
LWC, g m^{-3}	n.a.	0.21	0.21	0.21	0.21	0.21
Δz, m	232	232	232	232	232	232
Type	n.a.	C	C	C	C	C/M
r_{eff}, μm	n.a.	6.0	6.3	6.3	6.1	5.8
τ_{sca}	14.64	n.a.	n.a.	n.a.	n.a.	14.64
β_{abs}, km^{-1}	4×10^{-4}	n.a.	n.a.	n.a.	n.a.	0.22
τ_{abs}	1×10^{-4}	n.a.	n.a.	n.a.	n.a.	0.02
τ_{ext}	14.64	11.99	11.46	12.52	13.03	14.67
ϖ	0.999993	1.000000	1.000000	0.999900	0.999900	0.996448
g	0.86	0.84	0.84	0.86	0.86	0.84
Albedo	0.839	0.539	0.526	0.461	0.471	0.556
Absorption, W m^{-2}	13.7	43.6	43.6	167.1	170.3	65.1
Transmission	0.135	0.430	0.444	0.387	0.374	0.389

Notation is the same as in Table 8, except that the solar zenith angle is now 25.4°.

Table 11. Comparison With Parameterizations for the Continentally Influenced Track (JDT178t)

Parameter	*Twomey et al.* [1984]	*Jones et al.* [1994]		*Feichter et al.* [1997]		This study
		N_d Calc	N_d Given	N_d Calc	N_d Given	
N_a, cm^{-3}	n.a.	2850	n.a.	n.a.	n.a.	2850
$m_{SO_4^{2-}}$, μg m^{-3}	n.a.	n.a.	n.a.	26.4	n.a.	26.4
m_{OC}, μg m^{-3}	n.a.	n.a.	n.a.	n.a.	n.a.	1.4
m_{BC}, μg m^{-3}	n.a.	n.a.	n.a.	n.a.	n.a.	1.4
N_d, cm^{-3}	985	375	985	403	985	985
LWC, g m^{-3}	n.a.	0.21	0.21	0.21	0.21	0.22
Δz, m	232	232	232	232	232	232
Type	n.a.	C	C	C	C	C/M
r_{eff}, μm	n.a.	5.8	4.2	5.5	4.1	4.1
τ_{sca}	21.74	n.a.	n.a.	n.a.	n.a.	22.06
β_{abs}, km^{-1}	1×10^{-3}	n.a.	n.a.	n.a.	n.a.	0.16
τ_{abs}	2×10^{-4}	n.a.	n.a.	n.a.	n.a.	0.04
τ_{ext}	21.74	12.22	16.34	14.48	19.97	22.10
ϖ	0.999989	1.000000	1.000000	0.999900	0.999900	0.998341
g	0.86	0.84	0.84	0.85	0.85	0.83
Albedo	0.877	0.544	0.617	0.495	0.561	0.642
Albedo increase, %	5	1	17	7	19	15
Absorption, W m^{-2}	14.5	43.5	42.9	178.6	202.8	96.9
Transmission	0.093	0.425	0.346	0.340	0.245	0.264

Notation is the same as in Table 8, except that the solar zenith angle is 25.4°.

N_d from *Jones et al.* [1994] and *Feichter et al.* [1997] are compared with our results and with extrapolations from the results of *Gillani et al.* [1995] and *Ferek et al.* [1998]. (Note that the extrapolations of the measurements of *Gillani et al.* [1995] and *Ferek et al.* [1998] are not necessarily valid for the high aerosol concentrations in this study. Nevertheless, we include them for the sake of comparison.) Our nearly linear relationship between N_d and N_a is similar in nature to that found in *Flynn et al.* [2000] and *Martinsson et al.* [2000], indicating the possibility for a higher N_d to N_a ratio than that commonly used in models in particular cases with high aerosol loadings.

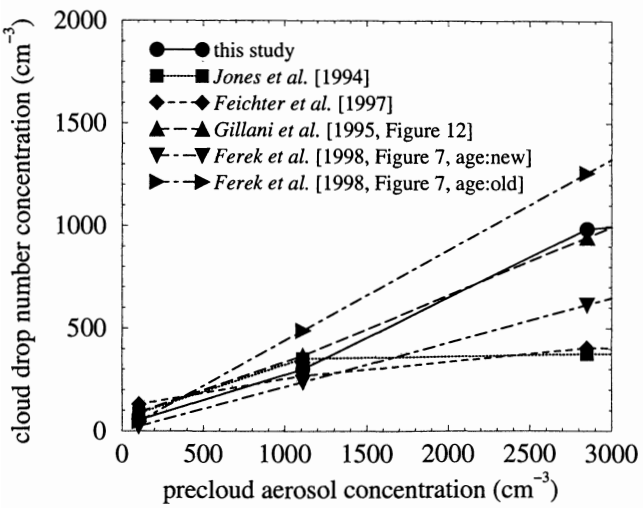

Figure 7. Relationship between cloud drop number concentration (N_d) and precloud aerosol concentration (N_a) from parameterizations, the model used in this study, and observations.

The issue of accurately parameterizing the relationship between cloud drop concentration and aerosol concentration, especially for large aerosol numbers, is complicated by measurement uncertainties. In heavily polluted situations such as ship tracks, the size range in which large numbers of activated particles typically fall can be problematic for instruments used to derive particle and cloud drop size distributions. Brenguier and colleagues have demonstrated that some cloud probes (including the Forward Scattering Spectrometer Probe (FSSP)) can have sampling errors at high droplet concentrations [*Brenguier and Amodei*, 1989; *Brenguier*, 1989, 1993; *Brenguier et al.*, 1998]. Similarly, the PVM-100 liquid water probe, used during the MAST campaign, can underestimate LWC by more than 50% by neglecting droplets less than ~1 μm [*Hobbs et al.*, 2000]. As one can see from the *Jones et al.* [1994] and *Feichter et al.* [1997] curves on Figure 7, empirical formulae based on such measurements tend to flatten out at cloud drop concentrations of ~350–400 cm^{-3}. Our model results, however, do not flatten out so quickly and fall within the extrapolations from *Gillani et al.* [1995] and *Ferek et al.* [1998]. Our model results also agree with measurements made during MAST. For example, in the continentally influenced track, FSSP counts (2–47 μm drops) were as high as 324 cm^{-3}, and Passive Cavity Spectrometer Probe (PCASP) (0.1–3.0 μm droplets) measurements were as high as 6532 cm^{-3} [*Noone et al.*, 2000b].

Because of the difficulty in parameterizing N_d, Tables 8-11 also contain columns labeled "N_d given," in

which the empirical formulae have been bypassed and N_d has been set to match our N_d. In these columns, there is better agreement in both r_{eff} and τ_{ext}, although there are still some remaining differences. One contributor to the remaining difference is the assumption in all of the parameterizations that the LWC is the same in the ambient cloud and ship track. In our model, the LWC tends to increase slightly from ambient cloud to ship track. This, in part, causes both *Jones et al.* [1994] and *Feichter et al.* [1997] to underestimate the τ_{ext} (except for Feichter et al.'s prediction of 23.45 for the clean marine track) and albedo of both ship tracks.

The remaining differences in r_{eff} may be attributed to the bulk representations *Jones et al.* [1994] and *Feichter et al.* [1997] used to calculate r_{eff}:

$$r_{\text{eff}} = \left(\frac{3\text{LWC}}{4\pi\kappa N_d}\right)^{1/3}, \tag{10}$$

where κ is 0.80 for maritime clouds and 0.67 for continental clouds. In contrast, we compute r_{eff} by integrating over the explicitly modeled size distribution according to the definition

$$r_{\text{eff}} = \frac{\int r^3 n(r) dr}{\int r^2 n(r) dr}. \tag{11}$$

The bulk representations of *Jones et al.* [1994] and *Feichter et al.* [1997] underestimate r_{eff} by 4–13% in the clean marine ambient cloud and track, while they overestimate r_{eff} by up to 9% in the continentally influenced ambient cloud and track.

Errors in the bulk representation of r_{eff}, however, tend to be compensated by the subsequent parameterizations of the extinction optical depth, single-scattering albedo (ϖ), and asymmetry factor. Again looking at the "N_d given" columns, *Jones et al.* [1994] and *Feichter et al.* [1997] predict 550 nm extinction optical depths which are very comparable to our extinction optical depths. The 0.3–3.0 μm albedos and the albedo increases are also comparable to our model results. *Jones et al.* [1994] predict albedo increases of 78 and 17% for the clean marine track and continentally influenced cloud track, respectively, while *Feichter et al.* [1997] predict albedo increases of 99 and 19%. Our modeled increases are 86 and 15%, respectively.

An additional source of error, which as in the *Twomey et al.* [1984] calculations manifests itself mostly in the absorbed irradiance, is the number of bands in the radiative parameterizations. The parameterization used by *Jones et al.* [1994], which is based on *Slingo* [1989], contains 24 bands, while the parameterization used by *Feichter et al.* [1997], which is based on *Boucher and Lohmann* [1995], is a simpler model containing only two bands. In contrast, our radiative parameters are computed from the Mie-scattering code (described earlier) in 53 bands, and these are subsequently averaged by the radiation algorithm into 26 bands. For *Feichter et al.* [1997] this creates a large discrepancy in their absorbed irradiance, since the single-scattering albedo for their 0.68–4.0 μm band is low (around 0.984), whereas a value of 0.999 or greater is more realistic from 0.68–1.2 μm. *Feichter et al.* [1997] overestimate the absorption by a factor of 2–5, lowering their albedo and transmission in all four cases. *Jones et al.* [1994] calculate a more reasonable absorption and transmission for the clean marine ambient cloud and track. However, because they assume pure water clouds, they underestimate the absorption in the continentally influenced cloud and track by 33–56%, and overestimate the transmission in both the ambient cloud and ship track. One can conclude from these comparisons that the major shortcomings of parameterizations lie in the empirical relationships between N_d and N_a, in the assumption that the LWC is held constant, in modeling size distribution changes whose subtleties are not captured by bulk parameterizations (e.g., r_{eff}), in using too broad a wavelength grid, and in assuming that clouds are composed of pure water.

In addition to the work of *Jones et al.* [1994] and *Feichter et al.* [1997], progress has been made toward developing prognostic treatments of cloud drop number in GCMs rather than using diagnostic empirical relationships [*Ghan et al.*, 1997; *Lohmann et al.*, 1999a,b]. Such treatments consider the influences of mixing and collision/coalescence as well as nucleation in determing cloud drop number. Because it is more difficult to predict the outcome of these prognostic schemes without doing an actual GCM simulation, which is beyond the scope of this paper, we do not attempt to assess these schemes here. However, we note that preliminary results show that using a mechanistic drop activation scheme, a higher cloud droplet/aerosol ratio is achieved than in the parameterizations of *Jones et al.* [1994] and *Feichter et al.* [1997] [*Penner*, 1999].

9. Summary

From our microphysical predictions of two ship track events from MAST, we find that ship track plumes in a clean marine stratocumulus and a continentally influenced marine stratocumulus increase the albedo and decrease the transmission of the clouds. While the albedo increase in the continentally influenced cloud is less than that in the clean marine cloud, making the continentally influenced cloud less susceptible, the increase in both cases is significant. Both clouds are found to increase atmospheric absorption above and within cloud level. The extra above-cloud absorption stems from the interaction between scattering off of the cloud top and absorption by O_3 and water vapor above the cloud, while the extra in-cloud absorption stems from the interaction between scattering by the cloud drops and absorption by water vapor and the drops themselves. In the clean cloud the drops absorb mostly in the near-infrared region because of their liquid water content, while in the continentally influenced cloud the drops also absorb in the ultraviolet and visible because of their dust and carbonaceous

content. Microphysical changes in cloud drop distribution and composition caused by aerosol pollution exert a substantive effect on the absorption of radiation above- and in-cloud such that there results a significant enhancement of atmospheric absorption.

Sensitivity studies were performed with respect to the updraft velocity, the updraft area fraction, dilution of the ship emissions, and the composition of supermicron continental particles. The explicit size distribution considerations reveal the possibilities of a nonmonotonic variation of the cloud drop number concentration and effective radius with respect to the updraft velocity depending on the air mass type in question. The albedo is most strongly influenced by changes in the updraft area fraction, where an increase in the updraft area fraction from 45 to 65% results in a 10–25% increase in albedo. The track albedo is also strongly influenced by dilution, where a 90% dilution of ship emissions reduces track albedo by 13–18%. The modeled albedos are shown to agree quite well with MRF C-130 albedo measurements as a function of track dilution, considering the uncertainties in calculated and measured values.

Our results are also compared with parameterizations of the "Twomey effect," where we find that the parameterizations tend to underestimate the albedo increase by underestimating the relationship between cloud drop number and aerosol number for large aerosol numbers. The parameterizations also underestimate the albedo increase by assuming that the LWC remains constant from ambient cloud to ship track. For the continentally influenced case the parameterizations tend to overestimate the albedo of both the ambient cloud and ship track because they neglect absorbing species within the cloud drops. In general, bulk parameterizations do not resolve the fine grain features revealed by explicit size distribution modeling, for example, the marked sensitivity to whether it is a maritime or continental airmass that is being polluted. The resolution of the model wavelength grid is also found to be an important factor, where only one or two bands in the infrared is insufficient to accurately resolve solar absorption.

Acknowledgments. We are grateful to Jonathan Taylor, MRF, for the broadband radiometer measurements, Ron Ferek, Dean Hegg, and Peter Hobbs, UW, for providing the aircraft measurements of SO_2 and the thermodynamic variables, and Phil Durkee and Kurt Nielsen, Naval Postgraduate School, for the AVHRR retrievals. We are also thankful to Doug Johnson, MRF, and Bjorn Stevens, Max Planck Institüt für Meteorologie, for their helpful discussions of updrafts and downdrafts, and Constantin Andronache, Will Cooke, Steve Klein, and Al Arking for their helpful comments on the manuscript. We thank Stuart Freidenreich for assistance with the shortwave algorithm. LMR acknowledges support from ONR grant N00014-97-1-0673.

References

Alkezweeny, A. J., D. A. Burrows, and C. A. Grainger, Measurements of cloud-droplet-size distributions in polluted and unpolluted stratiform clouds, *J. Appl. Meteorol., 32*, 106–115, 1993.

Bazhenov, O. E., E. I. Kas'yanov, and G. A. Titov, Influence of aerosol on mean albedo and absorption by broken clouds, *Atmos. Oceanic Phys., 30*(3), 300–307, 1994.

Bigg, E. K., J. L. Gras, and D. J. C. Mossop, Wind-produced submicron particles in the marine atmosphere, *Atmos. Res., 36*, 55–68, 1995.

Bohren, C. F., and D. R. Huffman, *Absorption and Scattering of Light by Small Particles*, John Wiley, New York, 1983.

Boucher, O., and U. Lohmann, The sulfate-CCN-cloud albedo effect, *Tellus, Ser. B, 47*, 281–300, 1995.

Bowyer, P. A., D. K. Woolf, and E. C. Monahan, Temperature dependence of the charge and aerosol production associated with a breaking wave in a whitecap simulation tank, *J. Geophys. Res., 95*, 5313–5319, 1990.

Brenguier, J.-L., Coincidence and dead-time corrections for particle counters, II, High concentration measurements with an FSSP, *J. Atmos. Oceanic Technol., 6*, 585–598, 1989.

Brenguier, J.-L., Observations of cloud microstructure at the centimeter scale, *J. Appl. Meteorol., 32*, 783–793, 1993.

Brenguier, J.-L., and L. Amodei, Coincidence and dead-time corrections for particle counters, I, A general mathematical formalism, *J. Atmos. Oceanic Technol., 6*, 575–584, 1989.

Brenguier, J.-L., T. Bourrianne, A. de Aeraujo Coehlo, J. Isbert, R. Peytavi, D. Trevarin, and P. Weschler, Improvements of droplet size distribution meausurements with the Fast-FSSP Forward Scattering Spectrometer Probe, *J. Atmos. Oceanic Technol., 15*, 1077–1090, 1998.

Brooks, I. M., and D. P. Rogers, Aircraft observations of boundary layer rolls off the coast of California, *J. Atmos. Sci., 54*, 1834–1849, 1997.

Cess, R. D., and M. H. Zhang, How much solar radiation do clouds absorb? (Response), *Science, 271*, 1133–1134, 1996.

Cess, R. D., et al., Absorption of solar radiation by clouds: Observations versus models, *Science, 267*, 496–499, 1995.

Collins, W. D., A global signature of enhanced shortwave absorption by clouds, *J. Geophys. Res., 103*(D24), 31,669–31,679, 1998.

d'Almeida, G. A., P. Koepke, and E. P. Shettle, *Atmospheric Aerosols: Global Climatology and Radiative Characteristics*, A. Deepak, Hampton, Va., 1991.

Durkee, P. A., R. E. Chartier, A. Brown, E. J. Trehubenko, S. D. Rogerson, C. Skupniewicz, K. E. Nielson, S. Platnick, and M. D. King, Composite ship track characteristics, *J. Atmos. Sci., 57*, 2542–2553, 2000a.

Durkee, P. A., et al., The impact of ship-produced aerosols on the microstructure and albedo of warm marine stratocumulus clouds: A test of MAST hypotheses 1.1a and 1.1b, *J. Atmos. Sci., 57*, 2554–2568, 2000b.

Evans, W. F. J., C. Reinhart, and E. Puckrin, A ground based measurement of the anomalous cloud absorption effect, *Geophys. Res. Lett., 22*(16), 2135–2138, 1995.

Feichter, J., U. Lohmann, and I. Schult, The atmospheric sulfur cycle in ECHAM-4 and its impact on the shortwave radiation, *Clim. Dyn., 13*, 235–246, 1997.

Ferek, R. J., D. A. Hegg, P. V. Hobbs, P. Durkee, and K. Nielsen, Measurements of ship-induced tracks in clouds off the Washington coast, *J. Geophys. Res., 103*(D18), 23,199–23,206, 1998.

Fitzgerald, J. W., and P. A. Spyers-Duran, Changes in cloud nucleus concentration and cloud droplet size distribution associated with pollution from St. Louis, *J. Appl. Meteorol., 12*, 511–516, 1973.

Flynn, M. J., et al., Modelling cloud processing of aerosol during the ACE-2 HILLCLOUD experiment, *Tellus, Ser. B, 52*, 779–800, 2000.

Freidenreich, S. M., and V. Ramaswamy, A new multiple band solar radiative parameterization for GCM's, *J. Geophys. Res.*, *104*(D24), 31,389–31,409, 1999.

Ghan, S. J., L. R. Leung, R. C. Easter, and H. Abdul-Razzak, Prediction of cloud droplet number in a general circulation model, *J. Geophys. Res.*, *102*(D18), 21,777–21,794, 1997.

Gillani, N. V., S. E. Schwartz, W. R. Leaitch, J. W. Strapp, and G. A. Isaac, Field observations in continental stratiform clouds: Partitioning of cloud particles between droplets and unactivated interstitial aerosols, *J. Geophys. Res.*, *100*(D9), 18,687–18,706, 1995.

Hale, G. M., and M. R. Querry, Optical constants of water in the 200-nm to 200-μm wavelength region, *Appl. Opt.*, *12*(3), 555–563, 1973.

Hänel, G., The properties of atmospheric aerosol particles as functions of the relative humidity at thermodynamic equilibrium with the surrounding moist air, *Adv. Geophys.*, *19*, 73–188, 1976.

Harshvardhan, W. Ridgway, V. Ramaswamy, S. M. Freidenreich, and M. Batey, Spectral characteristics of solar near-infrared absorption in cloudy atmospheres, *J. Geophys. Res.*, *103*(D22), 28,793–28,799, 1998.

Hildemann, L. M., G. R. Markowski, and G. R. Cass, Chemical composition of emissions from urban sources of fine organic aerosol, *Environ. Sci. Technol.*, *25*, 744–759, 1991.

Hobbs, P. V., et al., Emissions from ships with respect to their effects on clouds, *J. Atmos. Sci.*, *57*, 2570–2590, 2000.

Houghton, J. T., L. G. M. Filho, B. A. Callander, N. Harris, A. Kattenberg, and K. Maskell, New York, *Climate Change 1995: The Science of Climate Change*, Cambridge Univ. Press, New York, 1996.

Jones, A., D. L. Roberts, and A. Slingo, A climate model study of indirect radiative forcing by anthropogenic sulphate aerosols, *Nature*, *370*, 450–453, 1994.

Joseph, J. H., W. J. Wiscombe, and J. A. Weinmann, The delta-Eddington approximation for radiative flux transfer, *J. Atmos. Sci.*, *33*, 2452–2459, 1976.

King, M. D., L. F. Radke, and P. V. Hobbs, Optical properties of marine stratocumulus clouds modified by ships, *J. Geophys. Res.*, *98*, 2729–2739, 1993.

Kondratyev, K. A., V. I. Binenko, and O. P. Petrenchuk, Radiative properties of clouds influenced by a city, *Atmos. Oceanic Phys.*, *17*(2), 122–127, 1981.

Kondratyev, K. A., V. I. Binenko, and I. N. Melnikova, On excessive cloud absorption of solar radiation in the visible region, *Dokl. Ross. Akad. Nauk*, *345*(6), 816–818, 1995.

Leaitch, W. R., G. A. Isaac, J. W. Strapp, C. M. Banic, and H. A. Wiebe, The relationship between cloud droplet number concentrations and anthropogenic pollution: Observations and climatic implications, *J. Geophys. Res.*, *97*(D2), 2463–2474, 1992.

Li, Z., and L. Moreau, Alteration of atmospheric solar absorption by clouds: Simulation and observation, *J. Appl. Meteorol.*, *35*, 653–670, 1996.

Li, Z., H. W. Barker, and L. Moreau, The variable effect of clouds on atmospheric absorption of solar radiation, *Nature*, *376*, 486–490, 1995.

Lohmann, U., and J. Feichter, Impact of sulfate aerosols on albedo and lifetime of clouds: A sensitivity study with the ECHAM4 GCM, *J. Geophys. Res.*, *102*(D12), 13,685–13,700, 1997.

Lohmann, U., J. Feichter, C. C. Chuang, and J. E. Penner, Prediction of the number of cloud droplets in the ECHAM GCM, *J. Geophys. Res.*, *104*(D8), 9169–9198, 1999a.

Lohmann, U., J. Feichter, C. C. Chuang, and J. E. Penner, Correction to "Prediction of the number of cloud droplets in the ECHAM GCM" by Ulrike Lohmann et al., *J. Geophys. Res.*, *104*(D20), 24,557–24,563, 1999b.

Martinsson, B. G., et al., Validation of very high cloud droplet number concentrations in air masses transported thousands of kilometers over the ocean, *Tellus, Ser. B*, *52*, 801–804, 2000.

McClatchey, R. A., R. W. Fenn, J. E. A. Selby, F. E. Volz, and J. S. Garing, *Optical Properties of the Atmosphere*, *AFCRL-72-0497*, Air Force Geophys. Lab., Hanscom Air Force Base, Mass., 1972.

Noone, K. J., et al., A case study of ship track formation in a polluted marine boundary layer, *J. Atmos. Sci.*, *57*, 2748–2764, 2000a.

Noone, K. J., et al., A case study of ships forming and not forming tracks in moderately polluted clouds, *J. Atmos. Sci.*, *57*, 2729–2747, 2000b.

Penner, J. E., Climate Forcing, paper presented at Tenth Conference on Atmospheric Radiation, Am. Meteorol. Soc., Madison, Wi., 1999.

Pilewskie, P., and F. P. J. Valero, Direct observations of excess solar absorption by clouds, *Science*, *267*, 1626–1629, 1995.

Pilewskie, P., and F. P. J. Valero, How much solar radiation do clouds absorb? (Response), *Science*, *271*, 1134–1136, 1996.

Platnick, S., and S. Twomey, Determining the susceptibility of cloud albedo to changes in droplet concentration with the Advanced Very High Resolution Radiometer, *J. Appl. Meteorol.*, *33*, 334–347, 1994.

Pueschel, R. F., C. C. V. Valin, R. C. Castillo, J. A. Kadlecek, and E. Ganor, Aerosols in polluted versus nonpolluted air masses: Long-range transport and effects on clouds, *J. Climate Appl. Meteorol.*, *25*, 1908–1917, 1986.

Radke, L. F., J. A. Coakley Jr., and M. D. King, Direct and remote sensing observations of the effects of ships on clouds, *Science*, *246*, 1146–1149, 1989.

Ramanathan, V., B. Subasilar, G. J. Zhang, W. Conant, R. D. Cess, J. T. Kiehl, H. Grassl, and L. Shi, Warm pool heat budget and shortwave cloud forcing: A missing physics?, *Science*, *267*, 499–503, 1995.

Ramaswamy, V., and M. M. Bowen, Effects of changes in radiatively active species upon the lower stratospheric temperatures, *J. Geophys. Res.*, *99*(D9), 18,909–18,921, 1994.

Ramaswamy, V., and S. M. Freidenreich, A high-spectral resolution study of the near-infrared solar flux disposition in clear and overcast atmospheres, *J. Geophys. Res.*, *103*(D18), 23,255–23,273, 1998.

Reisin, T., Z. Levin, and S. Tzivion, Rain production in convective clouds as simulated by an axisymmetric model with detailed microphysics, I, Description of the model, *J. Atmos. Sci.*, *53*, 497–519, 1996.

Russell, L. M., and J. H. Seinfeld, Size- and composition-resolved externally-mixed aerosol model, *Aerosol Sci. Technol.*, *28*(5), 403–416, 1998.

Russell, L. M., S. N. Pandis, and J. H. Seinfeld, Aerosol production and growth in the marine boundary layer, *J. Geophys. Res.*, *99*(D10), 20,989–21,003, 1994.

Russell, L. M., R. C. Flagan, and J. H. Seinfeld, Asymmetric instrument response due to mixing effects in DMA-CPC measurements, *Aerosol Sci. Technol.*, *23*(4), 491–509, 1995.

Russell, L. M., S.-H. Zhang, R. C. Flagan, J. H. Seinfeld, M. R. Stolzenburg, and R. Caldow, Radially classified aerosol detector for aircraft-based submicron aerosol measurements, *J. Atmos. Oceanic Technol.*, *13*(3), 598–609, 1996.

Russell, L. M., et al., Aerosol dynamics in ship tracks, *J. Geophys. Res.*, *104*(D24), 31,077–31,095, 1999.

Slingo, A., A GCM parameterization for the shortwave radiative properties of water clouds, *J. Atmos. Sci.*, *46*, 1419–1427, 1989.

Stevens, B., W. R. Cotton, G. Feingold, and C.-H. Moeng, Large-eddy similations of strongly precipitating, shallow, stratocumulus-topped boundary layers, *J. Atmos. Sci.*, *55*, 3616–3638, 1998.

Tang, I. N., and H. R. Munkelwitz, Water activities, densities, and refractive indices of aqueous sulfates and sodium nitrate droplets of atmospheric importance, *J. Geophys. Res.*, *99*(D9), 18,801–18,808, 1994.

Taylor, J. P., and A. McHaffie, Measurements of cloud susceptibility, *J. Atmos. Sci.*, *51*, 1298–1306, 1994.

Taylor, J. P., J. M. Edwards, M. D. Glew, P. Hignett, and A. Slingo, Studies with a flexible new radiation code, II, Comparisons with aircraft short-wave observations, *Q. J. R. Meteorol. Soc.*, *122*, 839–861, 1996.

Taylor, J. P., M. D. Glew, J. A. Coakley, Jr., W. R. Tahnk, S. Platnick, P. V. Hobbs, and R. J. Ferek, Effects of aerosols on the radiative properties of clouds, *J. Atmos. Sci.*, *57*, 2656–2670, 2000.

Toon, O. B., J. B. Pollack, and B. N. Khare, The optical constants of several atmospheric aerosol species: ammonium sulfate, aluminum oxide, and sodium chloride, *J. Geophys. Res.*, *81*(33), 5733–5748, 1976.

Twohy, C. H., P. A. Durkee, B. J. Huebert, and R. J. Charlson, Effects of aerosol particles on the microphysics of coastal stratiform clouds, *J. Clim.*, *8*, 773–783, 1995.

Twomey, S. A., Pollution and the planetary albedo, *Atmos. Environ.*, *8*, 1251–1256, 1974.

Twomey, S. A., M. Piepgrass, and T. L. Wolfe, An assessment of the impact of pollution on global cloud albedo, *Tellus, Ser. B*, *36*, 356–366, 1984.

Weast, R. C., M. J. Astle, and W. H. Beyer (Eds.), *CRC Handbook of Chemistry and Physics*, 66th ed., CRC Press, Boca Raton, Fla., 1985–1986.

Wiscombe, W. J., and J. W. Evans, Exponential-sum fitting of radiative transmission functions, *J. Comput. Phys.*, *24*, 416–444, 1977.

C. Erlick, Ring Department of Atmospheric Sciences, The Hebrew University of Jerusalem, Jerusalem 91904, Israel. (caryn@sharav.es.huji.ac.il)

L. M. Russell, Department of Chemical Engineering, Princeton University, A317 Engineering Quadrangle, Princeton, NJ 08544. (lrussell@princeton.edu)

V. Ramaswamy, Geophysical Fluid Dynamics Laboratory, Princeton University, Forrestal Campus, U.S. Route 1, Princeton, NJ 08542. (vr@gfdl.gov)

(Received December 31, 1999; revised August 21, 2000; accepted August 29, 2000.)